# A practice-oriented model for pushover analysis of a class of timber-framed masonry buildings

**Leonidas Alexandros S. Kouris[a,1]*, Andreas J. Kappos[b]**

a - Former PhD student, Aristotle University of Thessaloniki, Department of Civil Engineering, Division of Structural Engineering, University Campus, 541 24 Thessaloniki, Greece; email: l.a.kouris@gmail.com

b - Professor, Department of Civil Engineering, City University London, EC1V OHB London, UK; email: Andreas.Kappos.1@city.ac.uk

**Abstract**

Timber-Framed (TF) masonry is a structural system characterized by high complexity and diversity. Limited experimental and analytical research has been carried out so far to explore their earthquake response, partly due to the complexity of the problem and partly due to the scarcity of TF buildings across the world. Here, a new practice-oriented non-linear (NL) macro-model is presented for TF masonry structures, based on the familiar diagonal strut approach with NL axial hinges in the struts. The constitutive law for the hinges (axial force vs. axial deformation) is derived on the basis of an extensive parametric analysis of the main factors affecting the response of TF masonry panels subjected to horizontal loading. The parameters studied are related to the geometric features of the panel and the strength of wood as well as the connections of the timber elements. The parametric analysis is performed using a micro-model based on Hill-type plasticity and it is shown that in the studied X-braced walls the masonry infills do not make a significant contribution to the lateral load resistance. Empirical expressions are proposed for the yield and maximum displacement and shear of a horizontally loaded TF panel. The model is verified against available experimental data, and is found to capture well the envelopes of the experimental loops. The model is readily applicable to NL static analysis (pushover) analysis for the assessment of the lateral load capacity of TF masonry buildings, as the number of input parameters for deriving the constitutive law has been limited to only five.

**Keywords: Timber-framed masonry, lateral load capacity, empirical macro-model, timber connections, pushover analysis, axial nonlinear hinges.**

[1] Present address: Rose School, IUSS Pavia, via Ferrata 1, 27100, Pavia, Italy.

## 1. Introduction

The last decade has witnessed an increased interest in TF structures, stimulated by reports on their relatively good performance during recent earthquakes. An interesting example are the 1999 Izmit and Ducze earthquakes in Turkey for which it has been argued [1,2] that TF masonry buildings performed better than not only conventional Unreinforced Masonry (URM) buildings, but even Reinforced Concrete (RC) buildings poorly detailed for seismic resistance. Indeed the implementation of a timber truss in the brickwork has its origin in the effort to tackle URM inefficiency against seismic loads. This truss that dates back to the 16th century B.C. in Greece [3] is sometimes so strong that TF structures are more of a timber structure than a URM one [4]. Using an X-bracing in a TF infilled panel (Figure 1) diminishes the role of masonry infills and lateral loads are carried by the main structural system which is the timber truss. From the ancient construction to contemporary TF systems such as those found in Pombalino buildings [5] a large variety of TF masonry walls is encountered, a key difference being the configuration of the wooden elements; herein the focus is on the bracing that is most effective for lateral load resistance, i.e. the cross-inclined diagonal (X-bracing).

### 1.1. Overview of available test results

Experimental research on this structural system has been quite limited, characterised by a growing interest in the last few years. It started in Portugal in 1997 [6]; this first experimental campaign involved three specimens extracted from an existing building in the historic centre of Lisbon. These TF walls were one storey high (3.5 m) and consisted of six X-braced panels. All joints between timber members were realized through iron nails and traditional carpentry joints that involved overlapping of the respective members; the diagonals were joined to the surrounding frame solely through nails, without any carpentry configuration. The walls were subjected to horizontal reversed cyclic loading at the top beam (without vertical load) and developed considerable ductility and energy dissipation capacity. Another finding of that research was that the initial elastic phase of the response was very brief, its end marked by un-nailing of the diagonals from the surrounding frame. Failure of TF walls was due to degradation of the frame, including partial out-of-plane failure of the masonry infills.

Recently, another series of TF walls were tested, also in Portugal [7]. This experimental research involved three large-scale specimens constructed in the laboratory that were shorter (2.6 m) than the ones taken from the old building. Joints were constructed as close as possible to those found in old buildings. A specific cyclic loading protocol appropriate for timber structures was used [8] involving both horizontal and vertical loading. Failure occurred due to out-of-plane falling of masonry infills and buckling of the diagonals. Test results confirmed the high displacement and energy dissipation capacity of TF walls; they also illustrated the pinching effect due to un-nailing of the diagonals and sliding of the

masonry infills. Meireles *et al.* [7] have also observed early detachment and low influence of masonry infills in the overall response of the TF walls.

Another experimental investigation, also conducted in Portugal, involved seven TF panels (1 m square) with diagonal braces [9]. Materials and construction techniques were similar to the previous test but with a view to rehabilitation and fast cure of masonry; to this end, cement-based mortar was used. The testing protocol was also similar. That study reconfirmed the key role of the diagonals and the early detachment of the masonry infills from the surrounding frame. Another interesting conclusion was that diagonals in tension separated from the surrounding frame at very small horizontal displacement. The authors suggested that the contribution of the infills should not be taken into account in analytical models.

Again, a cyclic horizontal force was applied and a constant vertical load to three full-scale walls (3 m long and 2.5 m high), each including 16 X-braced TF panels [10], a configuration common in areas of India and Pakistan (where the tests were carried out). However, joints were constructed using a different technique the mortise (groove) and tenon scheme, supplemented with mild steel nails, commonly used in TF structures in these areas, which is highly dependent on the axial load of the columns. The conclusions drawn are generally similar to those of the Portuguese researchers, i.e.: (a) highly NL response of the walls with separation of the connections under tensile stress, (b) minor contribution of the masonry infills to lateral stiffness and strength but rather important contribution to energy dissipation, and (c) rocking response due to the mortise and tenon joints.

### 1.2. Overview of available analytical models

Simplified models for TF structures have been confined so far mainly to elastic ones. The progressive removal of the failed elements from the model proposed by Cardoso *et al.* [11] is an approximate procedure, not particularly accurate in the estimate of displacements and not particularly convenient for every-day analysis since multiple runs with changing models are required; however, it has the advantage that there is no need for a proper nonlinear model. Masonry infills were ignored in the simulation and diagonal struts were assumed pinned at the connections and carrying compression only.

A similar approach is suggested by Vintzileou *et al.* [12] focusing on possible variations of the damaged structure and the collapse mechanism; it suffers from the same disadvantages regarding displacements. A distinction is made regarding the connections of timber elements; rigid connections are assumed between timber posts and beams, while the diagonals are taken as pinned to the surrounding timber frame.

Similarly, Ferreira *et al.* [9] assumed carpentry joints to be rigid and diagonals to be pinned at the connections. These authors presented a model comprised of beam, strut and plane elements. However, they found rather unrealistic results when they included masonry infills in the model, and decided to finally exclude them. A trial and error modification of the

stiffness of the diagonals was deemed necessary to achieve reasonable match with test results. A high modification factor (over 35) was proposed for reducing the axial stiffness; it should be noted that this modification factor applies specifically to the series of specimens considered in the study.

A NL macro-model was proposed by Ahmad *et al.* [10] for the previously described type of TF that is found in parts of Pakistan and India on the common lumped plasticity beam-column elements. Despite observing in their tests that inelastic deformation occurs mainly in the diagonals, they assigned NL hinges only to timber posts, while beams and diagonals were assumed to behave elastically. The inelastic law of the NL hinges involved both moment-rotation and axial force-axial deformation. The moment-rotation law was based on a bilinear approximation of the flexural strength vs. deformation curve of URM walls. The axial force-axial deformation law was also a bilinear approximation, this time of the axial strength vs. deformation curve of the timber posts. Based on test results they proposed two versions of their macro-model, a bilinear and a trilinear one, whose properties were defined through calibration against experimental results. Therefore, the use of this model is restricted to the type of walls studied in [10].

Another macro-model appropriate for response-history dynamic analysis of historic TF structures consists of a hysteretic model for the joints between posts and beams [13]. This model was initially developed for modern timber shear walls sheathed with plywood board (see for example [14]) and later adopted to traditional TF walls. This model excludes masonry infills and takes them into account indirectly, through the rotational springs that simulate the pinching effect during the reversal of the load direction. A methodology applied in six steps can estimate the maximum PGA that a structure can sustain and the behaviour factor q, provided that experimental results for TF walls are available to calibrate the model. A hysteretic model with exponential ascending and descending branches has been used for the analysis of traditional TF structures [7] although it has been originally developed for modern timber shear wall (see for example [15]). A step-by-step procedure for the calibration of the parameters of the hysteretic model has also been proposed [16].

Masonry infills are considered rigid and a set of elastic springs join the blocks to the timber structure to simulate the friction in an investigation of TF stone masonry walls without diagonals [17]. The mechanical characteristics of the materials are defined after a validation procedure against the available experimental results.

### 1.3. Objectives and scope

The main goal of this research is to provide a simple, and as general as possible, model for the analysis of TF buildings braced with ‘St Andrews’ diagonals. Using a micro-model previously developed by the authors [18], a systematic parametric analysis of TF panels is carried out to identify the main parameters that influence the seismic behaviour (*response parameters*). To derive relationships *response parameters* are considered independent from

each other; hence, empirical expressions are derived by means of least square fitting of the results of the parametric study. Each empirical expression characterizes a *response parameter* in terms of the pertinent *independent input parameters*. The guiding principle in formulating this empirical model was to include only the terms necessary for describing the kinematics of the TF panels (i.e. the *response parameters*). Applying those equations, it is possible to obtain the NL law for point plastic hinges used in the macro-model.

Based on this conceptual approach, the input of the proposed analytical model involves only the key geometric characteristics of the timber panels and the timber strength, all of which are easy to determine. Thus, the approach is practical and versatile in engineering applications. It can be used to assess the seismic behaviour of TF masonry buildings in terms of their pushover curves, and is deemed as a useful tool for seismic vulnerability and risk analyses.

## 2. Salient features of the seismic behaviour of TF masonry panels

Referring to the partially plastered TF masonry infilled wall of Figure 1, loaded with a horizontal force V at its top beam, its response is characterised by four distinct phases. Following a brief elastic phase, some cracks appear especially in the region of the diagonal braces; these are visible if stucco or plaster do not conceal them. The origin of this cracking is the initiation of relative sliding between masonry infills and diagonal braces. Hence, the first two phases are essentially elastic, i.e.: (i) the linear elastic phase during which no damage appears and (ii) the non-linear elastic phase subsequent to the aforementioned cracking. It is notable that this elastic stage constitutes a very small part of the total response either in terms of force or of energy absorption (and dissipation, when cyclic loading is applied).

An important change in the structural system occurs at the third stage manifested by the separation of the brace in tension from the surrounding frame. The shear force in the wall will continue to increase, but the response will be non-linear inelastic. The detached diagonal will remain unloaded and shear will be resisted by the compressed diagonal and to a lesser extent by the interface shear stresses developed between the diagonals and the sliding masonry infills. The fraction of the horizontal force carried by the shear mechanism of the infills is further examined in the following.

After detachment of the tension diagonal the panel will undergo large deformations. In this regard masonry infills serve essentially as lateral support for the timber elements and prevent, up to a certain extent, out-of-plane buckling of the diagonals in compression. As horizontal displacement of the panel increases, the gap between the tension diagonal and the frame becomes larger and masonry infills are no more able to deform, hence crush and eventually collapse out-of-plane. This is followed by visible buckling (and crushing) of the diagonals and leads to collapse, at the end of the final phase of the response.

In view of the above, it is clear that apart from the first elastic phase of the response, which is brief compared to the full range of response and negligible in terms of energy dissipation (hence of seismic resistance), the governing element of the X-braced panel in all other phases is the compression diagonal, whereas masonry infills play (prior to their failure) a positive, yet secondary, role. It has to be noted here that in other configurations of TF masonry, especially those that do not include proper diagonal elements, the role of masonry infills is more significant.

## 3. Analysis using the micro-model approach

### 3.1. Brief description of the micro-model

The parametric analysis is performed using a detailed plasticity-based finite element model previously developed by the authors [18]. In this model NL behaviour of timber elements is described by a Hill plasticity model for orthotropic materials [19, 20]. Isotropic hardening occurs for natural species of wood and is considered here to occur at a stress corresponding to 40% of its strength. The response of timber in uniaxial stress is assumed trilinear [21-23]; the second branch has modulus of elasticity equal to 10% the initial one, while the third branch is horizontal (fully plastic behaviour).

The response of a TF masonry panel (especially of the type found in traditional buildings) is highly affected by the inadequate detailing of the connection between the diagonal braces and the surrounding timber frame; this results to un-nailing of the iron nails, quite visible in the tests described in §1.1. Therefore, proper modelling of the joints should capture their opening and sliding, as well as the transmission of compressive and (interface) shear stresses. A simple contact is considered based on a friction-only constitutive law for the shear stress at the contact areas $\tau = \mu_f \cdot \sigma,$ where $\mu_f$ is the friction coefficient for isotropic friction, and $\sigma$ is the normal stress at the friction area.

The connection of the timber beams and timber posts and the connection of the diagonals are materialised through T-shaped lap carpentry joint (Figure 2) and two iron nails. In some cases the connection of the diagonals is not through carpentry joints but one diagonal is compact (i.e. one element) while the second consists of two separate parts (two elements). This detailing is typically associated with lower quality of construction. The T-shaped lap carpentry connection strengthened by iron nails is close to a monolithic, i.e. moment-resisting connection. Nevertheless, carpentry connections are rarely constructed with perfect fitting between their parts and some rotation of the joint should be expected. For simplicity and in view of the scarcity of available experimental data, this connection is considered here as rigid.

3.2. Influence of the connection of the diagonals

The influence of the connection between the diagonals is investigated comparing three different configurations (Figure 3) for a TF masonry panel that is loaded with a horizontal force (Figure 1). In this regard Figure 3a presents a TF panel with rigid connection between its diagonals, while Figure 3b and 3c have a contact surface for the tension and the compression diagonal, respectively; hence two bounding cases (full connection and simple contact) are studied. This investigation is carried out without considering the masonry infills for the effect of the connection to be clearer; however, the weight of the infills is taken into account. The dimensions of the TF panels are 2.0 m × 1.7 m × 0.1 m and the section of timber elements is 0.10 m × 0.10 m. Apart from the self-weight of the materials which is assumed $\rho_w$=350 kg/m$^3$ for wood and $\rho_m$=2000 kg/m$^3$ for masonry, an additional vertical load is applied representing the permanent and live loads of the floors and the superstructure; this is 8.4 kN in each of the posts and a uniformly distributed 5 kN/m vertical load on the upper beam. The mechanical properties for timber adopted here correspond to pine wood classified as C24 (24MPa) category in EN338 [24]. The compressive capacity of pine wood should be reduced to $f_{c,0,k}$= 18.9 MPa in the direction of the fibres and to $f_{c,90,k}$ = 4.7 MPa in the perpendicular direction taking into account the effect on the strength of the duration of the load and the moisture content in the structure. Tensile strength is considered equal to the compressive one. The modulus of elasticity in the direction of fibres is $E_{0,mean}$= 11 GPa and perpendicular to them $E_{90,mean}$= 0.37 GPa. Results in terms of shear (V) versus displacement of the top beam edge (Δ) are presented in Figure 4. It is clear that differences are negligible; the maximum difference in the shear resistance is less than 0.5% and in maximum displacement approximately 6%. The assumption of rigid connection gives shear resistance and displacement in-between the results from the other two assumptions (discontinuities). Consequently, the panel used in the parametric analysis could simply have rigid connection between the two diagonals since this: (i) is the most usual case, (ii) has negligible differences with respect to the models wherein discontinuities are included, and (iii) involves less computational effort.

The shear force $V_{pin}$ that would sustain an equivalent panel with pinned joints at the ends is equal to $N \cdot cos(tan^{-1}(1.7/2))$. Considering the diagonal as a rod with the aforementioned compressive strength, its axial capacity would be $N = 18.9 \cdot 10^3 \cdot 0.1 \cdot 0.1 = 189$ kN. Consequently, the shear force in the panel would be $V_{pin}$ = 144 kN. The ratio of the maximum shear force $V_{max}$ that the panel can resist (16.82 kN) and the shear force $V_{pin}$ that would carry the equivalent pin-ended panel is $V_{max}$ / $V_{pin}$ = 12%. This should be attributed to the outward deflection of the diagonals when experiencing out of plane buckling, which also takes place in reality as the experimental results suggest [25]. Hence, the eccentric axial compression along with the shear deformation and the sliding that occurs at the end of the compressed diagonal, as well as the reduced strength of the wood perpendicular to the fibres, cause a significant drop in the horizontal resistance of the panel.

3.3. Influence of masonry infills on the behaviour of TF panels

A common damage type observed in TF masonry buildings after earthquakes is sliding of masonry infills along timber elements which can lead up to their crushing and out-of-plane failure. The influence of masonry infills is investigated here on a panel with the geometric, material and load parameters of the analysis presented in § 3.2. Traditional TF buildings almost invariably have masonry infills of low strength and stiffness. Values for the modulus of elasticity *E* adopted in the literature vary widely: 0.15 GPa [11], 0.4 GPa [9], 0.77 GPa [7], 1.5 GPa [12], 3 GPa [26] up to 4.3 GPa [27]. Not all these values should be considered as thoroughly supported, nor have all of them been experimentally determined, nevertheless they reflect the experience (and judgement) of the researchers that put them forward. As an example, the value for *E* proposed in [9] would be expected to be higher than that indicated in [7] given the materials used. This large variability is an indication of the variability of masonry material used as infill over the years, all sorts of which can be classified as rather flexible and as such, serve (at least) the purpose of increasing the deformation capacity of the panel. Moreover, the value of the modulus of elasticity should also take into account a certain degree of cracking in the usual case that masonry infills are modelled as elastic. This assumption is made on the basis of both its low degree of activation (which will be confirmed in the following) and in order to have a clearer picture of the influence of *E* of the masonry infills on the behaviour of TF panels under horizontal loading.

The FE modelling of the TF panel is presented in Figure 5. The model was implemented in [28]. In this modelling approach, plane stress analysis was selected and the element Plane 182 was chosen which is able to handle orthotropic material properties; the selective reduced integration method [29] was selected for this element. The material was specified to be orthotropic and was assigned a plasticity law using the HILL and MISO options, respectively. For the contact surfaces (which are reduced to lines for the plane stress approach) the elements TARGE 169 and CONTA 171 were used. Asymmetric contact was selected. The nodes at the base are fixed (i.e. no translation in x, y directions). The application of the load is displacement controlled to ensure stability of the analysis and is applied at all top nodes. In Figure 5 these contact lines between diagonals and the surrounding frame, and masonry infills and timber elements, are indicated by a red solid line. For these contact lines friction coefficient $\mu_f$ is taken equal to 0.50 [30, 31]. More details of the FE modelling adopted, regarding the techniques of the analysis and justification of the aforementioned selections are provided in [31]. Analysis is terminated when singularities appear in the stiffness matrix due to development of excessive plastic strain, which do not permit its inversion and failure is assumed to occur at this stage.

Results of the NL static (pushover) analysis of the TF panel in terms of Von-Mises stress intensity as well as the final deformed shape are presented in Figure 6. High stresses develop in only the diagonal in compression and its edges develop plastic deformation. Flexural response of the frame is far less noticeable than the diagonal compression. Masonry infills

develop (Figure 6) low stresses which should not come as a surprise due to their initial detachment from the bounding timber elements. Only shear stresses are induced in masonry infills while they slide (with friction) along timber elements. As noted in the introductory section, their early sliding has been observed both experimentally [9] and analytically [11, 31]. Pushover curves from the analyses of the TF panels with various values of *E* for their masonry infills are summarised in Figure 7. Also included in the figure is the case of the bare TF panel which can be considered as the *E*=0 case. Consequently, for masonry infills with widely varying *E*, panel displacements remain almost unaffected and only the lateral load capacity of the panel displays a small increase with *E*. The initial stiffness of the panels is almost the same in all cases, since the discontinuities between timber elements and masonry infills, mean that the latter are only activated after some horizontal displacement of the panel; subsequent stiffness changes in proportion to lateral strength.

It is clear that the above differences in the shear strength of the panel (less than 6%) are negligible for a material like TF masonry which presents substantial variability in the characteristics of its constituent materials. Moreover, simplification of analysis by neglecting masonry infills is an important advantage, hence in the subsequent development of the macro-model masonry infills are not considered as a significant input parameter that may affect the response of TF panels.

### 3.4. Effectiveness of connection between beams and posts

In the analyses presented in the preceding paragraphs the connection between beams and posts has been considered rigid, i.e. the nodes of the finite elements of a beam are shared by the respective post. Thus, the joint formed by a beam and a post deforms as a frame joint. However, in existing TF masonry buildings, carpentry connections between beams and posts are not always implemented, and when implemented they are rarely constructed with perfect fitting, thus allowing some relative rotation between beams and posts at their connections. To study this feature, the parametric analysis in this paragraph considers a horizontal gap (with no initial width) between the beams and the posts. Only the outer nodes of the posts are connected to the corresponding nodes of the beams (nodes coincide) to allow for rotation about the external node. This is shown in Figure 8a where the nodes about which there is the possibility of rotation are denoted by a black bullet. It should be noted that the rotation is free only in the plane of the timber frame. In the transverse direction interfaces between posts and respective beams are furnished with contact elements to ensure the smooth transfer of vertical loads. An elastic spring connects the nodes of the beam and the respective post of the inner nodes of the joints (indicated by a spline in Figure 8a). The influence of the spring stiffness is examined in a panel with the geometric, material and load parameters of the analysis presented in §3.2. Six cases are analysed; apart from the model without springs, four cases with varying stiffness of the connecting spring from K= $10^2$ kN/m up to $10^5$ kN/m are investigated. The additional contact surfaces are simulated using the same contact elements as in §3.2. Coupling of the

horizontal degree of freedom between the corresponding nodes of beams and posts attached to the joint interface is enforced, to permit the transfer of shear force from the beam to the posts. The spring is realized with an elastic 'COMBIN 14' axial spring constrained to act only in the vertical direction.

Pushover curves for the TF panels with various joint connections are summarised in Figure 8b. Results show that key parameters such as yield and maximum shear capacity and yield displacement are only slightly affected by the various flexibility conditions studied. Nevertheless, connection flexibility has a non negligible effect on ultimate displacement. Indeed, the ultimate displacement for the free-to-rotate model as well as for the models with relatively low spring stiffness (K = $10^2$ kN/m and $10^3$ kN/m) is 0.023 m, whereas the ultimate displacement for the high spring stiffness (K = $10^4$ kN/m and $10^5$ kN/m) is equal to that of the rigid joint model (0.032 m). Therefore, a loose connection decreases the ultimate displacement by up to about 30% for common values of permanent loads.

For the sake of completeness, the parametric analysis is repeated this time without any vertical loading on the frame. This extreme case is not found in real structures since even the top floor carries the non negligible self-weight of the roof. Apart from the lack of vertical loading, all other geometric and material parameters remain the same. Results are presented in Figure 8c whence the following conclusions are drawn: the maximum forces practically do not change except in the case of the 'free to rotate' model; moreover the 'free to rotate' without vertical loads model shows smaller maximum displacement than the respective model with loads which should be attributed to numerical instabilities rather than the actual situation and thus, these results are not deemed as the real final state; the flexible spring (K = $10^2$ kN/m) leads to unrealistic values for displacement due to excessive rotation and deformation of the elements between the one-node-to-one-node element connections (nodes denoted by black bullet in Figure 8a); on the contrary for the stiff spring (K = $10^5$ kN/m) the maximum displacement becomes smaller when there is no vertical loading as the stiffness of the spring is very high and becomes the centre of rotation which leads to excessive deformation of the respective elements (Figure 9) and rather early termination of the analysis. The general trend is a logarithmic relationship between the stiffness of the springs and the change of the maximum displacements when the frame carries no vertical loading (Figure 10).

## 4. Parametric NL analysis of TF masonry panels

### 4.1. Design of the parametric study

Several finite element analyses were carried out to study the main parameters affecting the response of TF masonry walls subjected to monotonic horizontal load. Then, best fit equations were established for the main input parameters required for the macro-model. The *independent (input) parameters*, identified from a series of preliminary analyses as those

having the largest influence on the seismic response of a TF wall, are summarised in Table 1 in terms of the height *H,* length *L,* axial load *P* on the posts, and the distributed (here considered as uniform) loading *p* on the span; *response* parameters are also given in this table. It should be noted that the thickness *w* of timber elements is assumed to coincide with the thickness of the panel, while the compressive strength of timber $f_{c,t}$ is assumed equal to the tensile strength. The definition of the dimensions *H, L, w* and *d* is shown in Figure 11.

Therefore, the problem that needs to be solved has a rank of correlation 6×6 between the *response parameters* $\Omega_i$ and the *input parameters* $\Lambda_i$. In other words, *response parameters* $\{\Omega_i\} = \{V_y, V_u, K_{el}, K_{inel}\ \delta_y, \delta_u\}$ and *input parameters* $\Lambda_i = \{A, H/L, w, d, f_{c,t}\}$ is a system $Y_{ij}\ \{\Omega_i\} = f(\Lambda_i)$ where $Y_{ij}$ is a 6×6 matrix. The key assumption is that each response parameter $\Omega_i$ is independent of the others which means $Y_{ij}$ is a diagonal matrix ($Y_{ii} = \Omega_i$ and $Y_{ij} = 0$) and consequently, $\Omega_i = f(A, H/L, w, d, f_{c,t})$. So, evaluation of each of the six input parameters (Table 1) is carried out independently from the others, which substantially simplifies the analysis. The investigation domain over each input parameter $\Lambda_i$ is determined as a range of values typically found in common buildings. Then, the influence of this parameter on the six response quantities is quantified. Practically, only four of the previous quantities are generally needed to express the seismic response of a TF panel. However, as it will be shown, some of them are also affected by other parameters not included in the above mentioned input parameters (Table 1) and so, they are not selected as representative quantities.

Reference values of the input parameters for the TF walls under examination were as follows:

1. Area *A* equal to 1.44 $m^2$ (1.2x1.2 panel)
2. Ratio *R* of the external dimensions *H/L* equal to 1.
3. Section of timber elements equal to 10×10 $cm^2$.
4. Strength of timber $f_{c,t}$ equal to 18.9 MPa.
5. Vertical loading, i.e. axial load *P* on the posts equal to 4.26 kN and uniform loading *p* on the TF walls equal to 5 kN/m.

In order to estimate yield displacement $\delta_y$, yield shear $V_y$ and elastic $K_{el}$ and post-elastic $K_{inel}$ lateral stiffness, an appropriate definition of the yield point is necessary. Indeed, the calculated pushover curves for the TF panels have been approximated by bilinear curves. This process is based on an energy balance, i.e. equating the areas above and below the bilinear curve with respect to the original pushover curve [32] retaining the first and the last point of the actual curve (Figure 12). Pushover analysis is performed using displacement control.

4.2. Parametric analysis for the panel area

Parametric analysis for the effect of the area *A* was carried out selecting eleven TF walls with *A* varying from 0.36 $m^2$ up to 6.76 $m^2$ (reference value 1.44); dimensions of the panel vary from *L = H = 0.6* m to 2.6 m corresponding approximately to one quarter of a storey height up to a full storey height. Figure 13 shows three different TF walls used in the parametric analysis; the two extreme cases with respect to their area and an intermediate one. Given that the section of the diagonal braces is kept the same (see §4.1) it follows that the panel with the minimum area (Figure 13a) is the one most densely reinforced with timber elements, the intermediate panel (Figure 13b) is a rather harmonious combination of masonry (not shown in the figure) and timber, while the panel with the maximum area (Figure 13c) looks poorly reinforced with timber elements. Figure 14 displays the variation of yield and maximum shear, elastic and post-elastic lateral stiffness, and yield and maximum displacement, with the area *A*. The horizontal shear at yield and failure decreases with *A* in an almost linear fashion. The same also holds for the elastic lateral stiffness and the yield displacement which decreases and increases, respectively, almost linearly with high correlation coefficient (higher than 80%). On the contrary, post-elastic stiffness changes with the area in a bilinear mode (Figure 14b); the boundary between the two regions is the intermediate area wall. The first region is characterised by a steep decrease of $K_{inel}$ with increasing *A*, whereas the second region has a smooth decrease which can also be assumed constant. Rather than reflecting an intrinsic characteristic of the panel, this behaviour is primarily controlled by the way the bilinear approximation is made (see Figure 12), in particular that no negative slopes are allowed. Regarding the variation of the ultimate displacement (Figure 14c), this is a parabolic function with its maximum close to the intermediate area wall. It is concluded that a harmonious combination of wood and masonry contributes to maximizing its displacement ductility (i.e. the ratio of failure to yield displacement), while a heavily or poorly reinforced (with timber elements) wall lead to lower ductility. An analogy can be recognised here with the influence of the reinforcement ratio on the ductility of reinforced concrete sections.

4.3. Parametric analysis for the aspect ratio

A similar parametric analysis is carried out for TF walls with aspect ratio *H/L* varying from 0.5 to 2.0 (reference value 1.0). Eleven walls are analysed which have the typical properties 1, 3, 4 and 5 of §4.1 and the resulting variation of the response variables is identified by means of a least squares regression analysis of the parametric analysis results. This regression gives fitting functions with high correlation factor, over 90% [31]. An example for the variation of yield $V_y$ and maximum $V_u$ shears with *H/L* is given in Figure 15. This variation, as well as the variation of lateral stiffnesses $K_{el}$ and $K_{inel}$ with *H/L*, is exponential. On the contrary, the variation of $\delta_y$ and $\delta_u$ displacements with *H/L* is linear.

4.4. Parametric analysis for the panel thickness

The parametric analysis for values of the thickness $w$ of the panel within a range from 0.1 m to 0.2 m (reference value 0.1 m) reveals a linear trend in the variation of shears $V_y$ and $V_u$ (Figure 16) and lateral stiffnesses $K_{el}$ and $K_{inel}$, while displacements $\delta_y$ and $\delta_u$ remain practically constant, with mean value of 1.03 cm and 8.91 cm, and standard deviations 0.03 cm and 0.60 cm, respectively [31]. This can be justified on the basis of the nature of the influence of $w$ on the strength and stiffness of the panel, i.e. the fact that in-plane displacements are not substantially affected by out-of-plane geometric properties.

4.5. Parametric analysis for the timber section depth

The reference panel in this investigation has dimensions 1.8 m ×2.0 m because of the increased thickness $w$ = 0.15 m and depth $d$. All timber members have the same cross section. The range of $d$ varies from 0.075 m to 0.20 m which are typical timber sections found in existing TF masonry structures. Regarding the effect of depth $d$ on the response parameters a similar trend is observed as with $w$, i.e. linear increase with increasing values of $d$, however, the elastic lateral stiffness $K_{el}$ remains almost constant with $d$ (Figure 17). This unexpected result stems from the way the bilinear approximation is made, i.e. in applying the equal area concept, the 'yield' point of the bilinear curve does not in principle represent the real onset of the NL response but it is always located beyond this point. The smoother the pushover curve the larger is the distance between the yield point and the real onset of yielding. Although elastic stiffness increases with increasing $d$ values the curvature of the pushover curve near the yielding area also increases and this results to practically constant values of $K_{el}$.

4.6. Parametric analysis for the timber strength

Ten TF panels with varying timber strength $f_{c,t}$ parallel to the grain from 16 MPa to 26 MPa were examined in the parametric analysis for the effect of strength. The compressive strength perpendicular to the fibres direction is equal to 25% and, thus, follows the same trend. Moreover, there is a corresponding variation of the elastic modulus [24], given in Table 2. The remaining input parameters were kept constant, the dimension of the panels being 1.3 m × 1.1 m. The shears $V_y$ and $V_u$ are linearly correlated to $f_{c,t}$ with correlation coefficient exceeding 90%. Also linear is the variation of lateral stiffnesses $K_{el}$ and $K_{inel}$. Timber strength does not affect displacements $\delta_y$ and $\delta_u$, which remain almost constant.

4.7. Parametric analysis for the vertical loading

Vertical loads $N$ acting on a TF panel originate from their self-weight of the structure and from permanent and live loading in the part of the structure above them. Self-weight is directly modelled but loads from the upper structure should be added to posts (axial forces of the upper storeys, $P$) and to the beams (vertical distributed loading from the floors, $p$). These two patterns constitute the external gravity load ($N_w$). Further contribution ($N_s$) to the

vertical loading of the TF panels is made by the overturning moment due to horizontal (seismic) loading of the structure. However, due to the reversed cyclic nature of the seismic action effects, on average the mean value of the total external axial load ($N$) is approximately equal to the one corresponding to gravity loads ($N_w$). Therefore, in the investigation of the vertical loading $N$ only equal loads are applied to both posts of a TF panel. The total vertical load varies from $N$ = 10 kN to 90 kN, retaining a 4:1 proportion between the concentrated and the distributed vertical loading.

The variation of shears at yield $V_y$ and failure $V_u$ with vertical load $N$ are presented in Figure 19. Both $V_y$ and $V_u$ slightly decrease with increasing vertical load. This negative slope of the V-N curves can be attributed to second order effects; however, the reduction of shears with the vertical load is rather negligible. Mean values for the entire range of considered vertical load are $V_u$ =12.13 kN and $V_y$ =9.53 kN whereas the corresponding COVs are 7.0% and 3.5%, respectively, i.e. very small. Consequently, in a practice-oriented model the influence of the vertical load on these parameters can be neglected.

Elastic lateral stiffness seems to be substantially influenced by the vertical load $N$ (Figure 19b); the linear correlation function has a negative slope $\tan(-83.93^0)= -9.40$. However, closer observation of the actual pushover curves shows that their initial stiffness does not change at the same rate but it is either constant or very slightly influenced by N. Again the bilinearization procedure affects the 'elastic' stiffness, while second order phenomena do not play such a substantial role in the elastic lateral stiffness. Post-yield stiffness remains practically constant with $N$ (Figure 19b).

Regarding the influence of the vertical load $N$ on yield displacement $\delta_y$ it remains almost constant around an average $\delta_y$ = 1.23 cm with a COV of 13%. On the contrary, maximum displacement $\delta_u$ (Figure 19c) is strongly influenced by the vertical load $N$. The mean value for maximum displacement $\delta_u$ is 7.89 cm with a COV of 28.5% which is comparatively high. It appears that there are two regions with an almost constant maximum displacement $\delta_u$; a region with low $N$ (<70kN) and a region with high $N$ (≥70kN) where a significant decrease in the maximum displacement $\delta_u$ has taken place; after the threshold of 70 kN the maximum displacement $\delta_u$ decreases substantially and then remains constant (Figure 19c).

## 5. Proposed empirical model

The findings of the foregoing parametric analysis are used to derive (through least square fitting) empirical relationships for the parameters required for defining the constitutive law of the macro-model.

5.1. Empirical expression for shear at yield

The main parameter affecting the shear $V_y$, as it is evident (and not surprising) from the above analysis, is the compressive strength $f_{c,t}$ of wood that defines the strength of the diagonal strut. The basic formulation of the expression for shear $V_y$ is as follows:

$$V_y = \lambda_{A,V_y} \lambda_{R,V_y} \lambda_{w,V_y} \lambda_{d,V_y} \lambda_{N,V_y} \cdot \phi_{V_y}(f_{ct}) \quad (1)$$

In Equation (1) $\lambda_{A,Vy}$ is a correction coefficient that takes into account the area of the panel, $\lambda_{R,Vy}$ is a correction coefficient that takes into account the aspect ratio $H/L$ of the of the panel, $\lambda_{w,Vy}$ is a correction coefficient that takes into account the thickness of the panel, $\lambda_{d,Vy}$ is a correction coefficient that takes into account the depth of the cross section of the timber elements, $\lambda_{N,Vy}$ is a correction coefficient that takes into account the vertical loading and $\varphi_{Vy}(f_{ct})$ is a function depending on the compressive strength $f_{c,t}$ of wood. It is pointed out that all correction coefficients are dimensionless. The function $\varphi_{Vy}(f_{ct})$ was found from linear regression to be (in kN):

$$\phi_{V_y}(f_{ct}) = 1.02 \cdot f_{ct} - 0.59 \quad (2)$$

where $f_{c,t}$ is the compressive strength of wood in MPa. The correction coefficient $\lambda_{N,Vy}$ may be taken equal to 1 and the remaining four should be estimated according to Figure 20.

5.2. Empirical expression for maximum shear

The shear strength $V_u$ is expressed by a similar empirical equation as for $V_y$ (which is set as a lower limit to $V_u$, to avoid negative slopes that create numerical problems):

$$V_u = \max \begin{cases} \lambda_{A,V_u} \lambda_{R,V_u} \lambda_{w,V_u} \lambda_{d,V_u} \lambda_{N,V_u} \cdot \phi_{V_u}(f_{ct}) \\ V_y \end{cases} \quad (3)$$

Again $\lambda_{i,Vu}$ are correction coefficients and $\varphi_{Vu}(f_{ct})$ is a function depending on the compressive strength $f_{c,t}$ of wood. Note that shears $V_y$ and $V_u$ may be very close to each other for some extreme cases of the geometry when displacement ductility is rather low.

The function $\varphi_{Vu}(f_{ct})$ is given by the following expression (in kN):

$$\phi_{V_u}(f_{ct}) = 1.31 \cdot f_{ct} + 0.03 \quad (4)$$

where $f_{ct}$ is the compressive strength of wood in MPa. The dimensionless correction coefficients should be estimated from Figure 21, while $\lambda_{N,Vu}$ can be taken equal to 1.

5.3. Empirical expression for yield displacement

Displacements are basically affected by the geometry of the panel; yield displacement $\delta_y$ is mainly affected by the area of the panel. The empirical formula to determine the yield displacement is given by:

$$\delta_y = \lambda_{R,\delta_y} \lambda_{d,\delta_y} \cdot \phi_{\delta_y}(A) \quad (5)$$

In Equation (5) $\lambda_{R,\delta y}$ is a correction coefficient that takes into account the aspect ratio of the panel, $\lambda_{d,\delta y}$ is a correction coefficient for the depth of the cross section of the timber elements, and $\varphi_{\delta y}(A)$ is a function depending on the area of the TF panel. This function $\varphi_{\delta y}(A)$ is given by the following expression (in cm):

$$\phi_{\delta_y}(A) = 0.03 \cdot A + 0.74 \quad (6)$$

where A is the area of the panel in $m^2$. The dimensionless correction coefficient $\lambda_{R,\delta y}$ should be estimated from Figure 22 and $\lambda_{d,\delta y}$ may be taken equal to 1 for usual values of *d* (see §4.5).

5.4. Empirical expression for maximum displacement

In section 4 it was found that maximum displacement is not only affected by the geometry of the panel but also from the vertical loading. The main parameter should be the aspect ratio of the panel. In section 3.2 was found that for loose woodworking of the carpentry joints the ultimate displacement decreases. The empirical relation to determine the maximum displacement is given by:

$$\delta_u = \max \begin{cases} \lambda_{\xi,\delta_u} \lambda_{A,\delta_u} \lambda_{d,\delta_u} \lambda_{N,\delta_u} \cdot \varphi_{\delta_u}(H/L) \\ 1.5 \cdot \delta_y \end{cases} \quad (7)$$

In Equation (7) $\lambda_{A,\delta u}$ is a correction coefficient that takes into account the area of the panel and should be estimated from Figure 23, $\lambda_{d,\delta u}$ is a correction coefficient for the depth of the cross section of the timber elements and may be taken equal to 1, $\lambda_{N,\delta u}$ is a correction coefficient for the vertical loading, and $\varphi_{\delta u}(H/L)$ is a function depending on the aspect ratio of the TF panel. This function $\varphi_{\delta u}(H/L)$ is given by the following expression (in cm):

$$\phi_{\delta_u}(H/L) = 10.56 \cdot H/L - 4.32 \quad (8)$$

the following two values are proposed for the $\lambda_{N,\delta u}$ correction coefficient:

$$\lambda_{N,\delta_u} = \begin{cases} 1, \ for \ \ p < 65kN/m \\ 0.5, \ for \ \ p \geq 65kN/m \end{cases} \quad (9a)$$

The correction coefficient $\lambda_{\xi,\delta u}$ assumes the value 0.75 when the fitting of the carpentry joint is loose or 1 when it is effective. In the extreme case of absence of any vertical loading for a frame connection with a rotational stiffness $K_\varphi$ (in kN/m/rad) the following empirical relation can be applied:

$$\lambda_{\xi,\delta_u} = 0.15\ln(K_\phi) - 0.7 \quad (9b)$$

It is recalled that the total vertical loading ($N$) consists of two parts, the axial loading on timber posts ($P$) and the uniformly distributed loading ($p$) on timber beams. In Equation (9) an equivalent uniformly distributed load ($p_{eq}$) on the span of length $L$ is used, as follows:

$$p_{eq} = p + \frac{2P}{L} \quad (10)$$

5.5. Implementation of the procedure

The proposed macro-model is implemented through the following steps:

1. Discretization of the building into individual TF panels.
2. The equivalent vertical load (equation 10) is calculated in each TF panel.
3. The empirical formulas (Equations 1 to 9) are applied to define the constitutive load of each panel in terms of horizontal shear vs. displacement.
4. The elastic stiffness of the diagonals (see Figure 11 for notation) is corrected using the following procedure [31]:

$$k_s = \frac{\left(H^2 + L^2\right)^{3/2} + H^3}{EF} \cdot \frac{1}{L^2} \cdot \frac{V_y}{\delta_y} \quad (11a)$$

where $E$ is the elastic modulus of wood (parallel to the grain) and $F$ is the diagonal's cross section.

The modified elastic modulus $E'$ is the product of correction coefficient $k_s$ and the elastic modulus and the resulting axial stiffness $K_{el}$ of the diagonal shall be:

$$K_{el} = \frac{\mathrm{E}'F}{\sqrt{H^2 + L^2}} = k_s \frac{\mathrm{E}F}{\sqrt{H^2 + L^2}} \quad (11b)$$

5. The NL law of the plastic hinges in the diagonal struts is defined in terms of axial load vs. deformation through the following expressions [18]:

$$N_{diag} = V\frac{\sqrt{H^2 + L^2}}{L},\ \mu_d = \frac{\delta_u}{\delta_y} = \frac{u_{diag,u}}{u_{diag,y}} \quad (12a)$$

$$u_{diag,y} = \frac{N_{diag,y}}{K_{el}} \quad (12b)$$

$$u_u = 1.2 \cdot u_{diag,\max}\ \ and\ \ N_{res} = 0.2 \cdot N_{diag,\max} \quad (12c)$$

In Equation (12) $u_u$ is the maximum axial deformation, $u_{diag,max}$ the axial deformation at maximum axial force, $N_{res}$ is the residual axial force after the drop in strength and

$N_{diag,max}$ is the maximum axial load, i.e. strength degradation takes place prior to the development of the ultimate displacement; $\mu_d$ is the displacement ductility, as well as the ductility in terms of axial deformation.

6. Pushover analysis of the structure consisting of the braced TF panels defined in the previous steps.

## 6. Verification of the model against experimental results

The procedure described in section 5.5 is applied to the experimental specimens tested at IST (Instituto Superior Técnico) Lisbon [7]. The discretization of the TF specimens into four panels is illustrated in Figure 24a (step 1). It is noted that the geometry is not exactly the same as that in the parametric analysis (Figure 11), since not all elements have the same thickness. For cases where there is small variation in *w* the following equation could be applied to estimate an equivalent thickness

$$w_{eq} = (A_{diag}w_{diag} + A_{col}w_{col} + A_b w_b + A_{inf}w_{inf}) / (A_{diag} + A_{col} + A_b + A_{inf}) \quad (13)$$

where the weighting coefficients $A_i$ are the area of the $i^{th}$ member (diagonals, columns, beams and infills respectively). Basic data of the specimens necessary to implement the model are presented in Table 3. The implemented loading protocol was that of CUREE [8]. The experimental setup is presented in Figure 26a. Further details on the experimental procedure can be found in [7]. The vertical load 30 kN/m equals to a total 76.8 kN. The empirical formulas applied at the third step would give:

From Equation (2) $\varphi_{V_y}\left(f_{ct}\right) = 1.02 \cdot f_{ct} - 0.59 = 1.02 \cdot 25 - 0.59 = 24.9kN$ (14)

Next, the correction coefficients are:

$$for\ A = 1.72m^2 \overset{Figure 18a}{\Rightarrow} \lambda_{A,V_y} = 0.97$$

$$for\ H/L = 0.98 \overset{Figure 18b}{\Rightarrow} \lambda_{R,V_y} = 1.18$$

$$for\ w = 0.10m \overset{Figure 18c}{\Rightarrow} \lambda_{w,V_y} = 0.67$$

$$for\ d = 0.10m \overset{Figure 18d}{\Rightarrow} \lambda_{d,V_y} = 1$$

$$\lambda_{N,V_y} = 1$$

Substituting Equation (14) and the above correction coefficients in Equation (1):

$$V_y = \lambda_{A,V_y}\lambda_{R,V_y}\lambda_{w,V_y}\lambda_{d,V_y}\lambda_{N,V_y} \cdot \varphi_{V_y}\left(f_{ct}\right) = 0.97 \cdot 1.18 \cdot 0.67 \cdot 1 \cdot 1 \cdot 24.9 = 19.13kN$$

From Equation (4) $\varphi_{V_u}\left(f_{ct}\right) = 1.31 \cdot f_{ct} + 0.03 = 1.31 \cdot 25 + 0.03 = 32.90kN$ (15)

Next, the correction coefficients are:

$$for\ A = 1.72m^2 \overset{Figure19a}{\Rightarrow} \lambda_{A,V_u} = 0.94$$

$$for\ H/L = 0.98 \overset{Figure19b}{\Rightarrow} \lambda_{\mathrm{R},V_u} = 1.19$$

$$for\ w = 0.10m \overset{Figure19c}{\Rightarrow} \lambda_{w,V_u} = 0.67$$

$$for\ d = 0.10m \overset{Figure19d}{\Rightarrow} \lambda_{d,V_u} = 1$$

$$\lambda_{N,V_u} = 1$$

Substituting Equation (14) and the above correction coefficients in Equation (3):

$$V_u = \max \begin{cases} \lambda_{\mathrm{A},V_u}\lambda_{R,V_u}\lambda_{w,V_u}\lambda_{d,V_u}\lambda_{N,V_u} \cdot \varphi_{V_u}\left(f_{ct}\right) = 0.94 \cdot 1.19 \cdot 0.67 \cdot 1 \cdot 1 \cdot 32.90 = 24.46kN \\ V_y = 18.96kN \end{cases} = 24.46kN$$

From Equation (6) $\varphi_{\delta_y}\left(A\right) = 0.03 \cdot A + 0.74 = 0.03 \cdot 1.72 + 0.74 = 0.78cm$ (16)

Next, the correction coefficients are:

$$for\ H/L = 0.98 \overset{Figure20}{\Rightarrow} \lambda_{\mathrm{R},\delta_y} = 0.88$$

$$\lambda_{d,\delta_y} = 1$$

Substituting Equation (16) and the above correction coefficients in Equation (5):

$$\delta_y = \lambda_{R,\delta_y}\lambda_{d,\delta_y} \cdot \varphi_{\delta_y}\left(A\right) = 0.88 \cdot 1 \cdot 0.78 = 0.69cm$$

From Equation (8) $\varphi_{\delta_u}\left(H/L\right) = 10.56 \cdot H/L - 4.32 = 10.56 \cdot 0.98 - 4.32 = 6.08cm$ (17)

Next, the correction coefficients are:

$$for\ A = 1.72m^2 \overset{Figure21}{\Rightarrow} \lambda_{A,\delta_u} = 0.90$$

$$\lambda_{d,\delta_u} = 1$$

$$\lambda_{\xi,\delta_u} = 1$$

$$for\ p \le 65kN/m \Rightarrow \lambda_{N,\delta_u} = 1$$

Substituting Equation (16) and the above correction coefficients in Equation (7):

$$\delta_u = \max \begin{cases} \lambda_{\xi,\delta_u}\lambda_{A,\delta_u}\lambda_{d,\delta_u}\lambda_{N,\delta_u} \cdot \varphi_{\delta_u}\left(H/L\right) = 1 \cdot 0.9 \cdot 1 \cdot 1 \cdot 6.08 = 5.46 \\ 1.5 \cdot \delta_y = 1.5 \cdot 0.69 = 1.04 \end{cases} = 5.46cm$$

The elastic stiffness of the diagonals is corrected (step 4) using Equations (11):

$$k_s = \frac{\left(H^2 + L^2\right)^{3/2} + H^3}{EF} \cdot \frac{1}{L^2} \cdot \frac{V_y}{\delta_y} = \frac{\left(1.3^2 + 1.32^2\right)^{3/2} + 1.32^3}{12 \cdot 10^6 \cdot 0.007} \cdot \frac{1}{1.3^2} \cdot \frac{19.13}{0.69 \cdot 10^{-2}} = 0.16$$

$$K_{el} = k_s \frac{\mathrm{E}F}{\sqrt{H^2 + L^2}} = 0.16 \frac{12 \cdot 10^6 \cdot 0.007}{\sqrt{1.3^2 + 1.32^2}} = 7390.66 kN / m$$

Then, Equations (12) are applied to specify the plastic hinge of the diagonals:

$$N_{diag,y} = V_y \frac{\sqrt{H^2 + L^2}}{L} = 19.13 \frac{\sqrt{1.3^2 + 1.32^2}}{1.3} = 26.85 kN$$

$$N_{diag,u} = V_u \frac{\sqrt{H^2 + L^2}}{L} = 24.6 \frac{\sqrt{1.3^2 + 1.32^2}}{1.3} = 34.53 kN$$

$$u_{diag,y} = \frac{N_{diag,y}}{K_{el}} = \frac{26.85}{7390.66} 10^{-2} = 0.36 cm$$

$$u_{diag,u} = \mu_d \cdot u_{diag,y} = \frac{\delta_u}{\delta_y} u_{diag,y} = \frac{5.46}{0.69} 0.36 = 2.89 cm$$

$$u_u = 1.2 \cdot u_{diag,\max} = 3.47 cm \ and \ N_{res} = 0.2 \cdot N_{diag,u} = 6.91 kN$$

The plastic hinge of the diagonal as defined using the proposed methodology is presented in Figure 25. The macro-model of the TF specimens is shown in Figure 24b. The green dots in the middle of the diagonals represent the plastic hinges. All members are pinned at their ends (black dots in Figure 22b). Base nodes have displacements fixed.

The yield shear resulting from the pushover analysis of the wall is 38.5 kN while the maximum shear is equal to 44.4 kN. The elastic lateral stiffness is 3256 kN/m and the maximum displacement is 9.5 cm which occurs when the wall carries the maximum shear.

Comparing the model with the envelope of the experimental loops (Figure 26b) it is seen that there is a reasonably good match between theoretical and experimental results, deemed sufficient for practical purposes. More specifically, for the first experimental cycle the experimentally measured secant lateral stiffness [33] at the yield point ($\delta_y$ = 1.2 mm) of the analytical model is 3798 kN/m for specimen SC2, while for specimen SC3 it is 3836 kN/m, which is 16% higher than the model stiffness, considered as a reasonable difference for a model aiming primarily at the NL response. The maximum shear for specimen SC2 is 48 kN and for SC3 is 51 kN, which are 9% and 16% higher than the strengths predicted by the model. The shear developed during the last loop before substantial degradation takes place is about 40 kN for either specimen, which is 10% less than the theoretical one.

Regarding displacements, the maximum value estimated by the analytical model is 9.5 cm, while the maximum experimental one is 9 cm for SC2 and SC3 for the last loop before the

substantial degradation in the shear resistance. Specimen SC3 reached an ultimate displacement of 12 cm but that corresponded to a shear near one third of the maximum.

As a further verification, the proposed model is applied to the specimens tested at LNEC (Portuguese National Laboratory for Civil Engineering), Lisbon [6]; details of their geometry and mechanical characteristics are given in [18]. During this experiment no specific loading protocol was implemented and there was no application of vertical loading. The test setup is shown in Figure 27a. The implementation of the model resulted in the pushover curves given in Figure 27 where a good match with the experimental envelopes of the loops is seen. Main results are summarised in Table 4. Comparing the analytical maximum shear against the test results there is difference from 5% to 12% with respect to the three test specimens, which is very similar to that noted with respect to the IST tests. The differences in terms of ultimate displacements may be up to 20% but the mean difference is 11% which is a relatively good estimate for a such an anisotropic and inhomogeneous material as TF masonry.

## 7. Conclusions

The key objective of the present study was to investigate the response of TF masonry panels submitted to lateral loads and to develop a simple NL model to be used in pushover analysis of realistically sized buildings with TF panels, requiring knowledge of as few input parameters as possible. The selected parameters depend only on TF panel geometry and the strength of timber, and were related through regression of the results of an extensive parametric study (using a refined finite element model previously developed by the authors) to the main quantities required to define the constitutive relationship of the TF walls in the 'practical' model; the relationship used in the model is the axial force vs. deformation of the hinges in the diagonal struts, wherein inelastic behaviour is expected. The proposed empirical relationships apply to X-braced TF walls, the configuration that is most efficient for earthquake resistance and can be used in pushover analysis. The contribution of masonry infills was also investigated (using the detailed finite element model) and found to be barely influential; hence they were neglected in the proposed macro-model. Moreover, the degree of the connection effectiveness between beams and post was investigated and found to affect substantially only the ultimate displacement of the panel.

The reliability of the proposed empirical model was validated using five TF wall specimens tested in two Portuguese laboratories. A reasonably good match of the envelopes of the experimental loops was found for both test series; the macro-model was able to capture the salient features of the response (strength, stiffness, ultimate deformation) within an accuracy that is deemed appropriate for practical analysis, especially if the significant uncertainties in the mechanical characteristics of this interesting, still complex, type of traditional structural system are considered.

The proposed macro-model permits estimation of the lateral load capacity of traditional TF buildings not only with relatively limited computational effort, but also with limited knowledge about the properties of the structure, which are not easy to define in an existing building, especially when this is a listed one. The procedure used herein can also be applied to study other configurations of TF masonry and develop ad-hoc empirical relationships. The proposed model should not be used for substantially different TF panel configurations, such as those without any diagonal braces.

**Acknowledgements**

The authors wish to thank Prof. Rita Bento and Dr. Helena Meireles from the Technical University of Lisbon (IST) for providing details of their experimental data. The author L.A. Kouris gratefully acknowledges the financial support provided by the Aristotle University of Thessaloniki for carrying out this work.

**References**

[1] Langenbach R. Survivors among the Ruins: Traditional Houses in Earthquakes in Turkey and India. APT Bulletin 2002;33(2/3):47-56.

[2] Şahin Güçhan N. Observations on earthquake resistance of traditional timber-framed houses in Turkey. Build.Environ. 2007;42(2):840-51.

[3] Palyvou C. The Akrotiri in Thera: The art of building, 1999 [in Greek].

[4] Tsakanika E. The structural role of timber in Palatial Architecture of Minoan Crete, PhD Thesis. Department of Architectural Engineering, National Technical University of Athens; 2006 [in Greek].

[5] Silva V, Lourenço PB, Ramos LF, Mesquita CG. Accounting for the “block effect” in structural interventions in Lisbon’s old “Pombaline” downtown buildings. Historical Constructions, Guimarães: University of Minho; 2001.

[6] Santos PS. Laboratory tests on masonry walls taken from an ancient building in Lisbon. 1997;17/97.

[7] Meireles H, Bento R, Cattari S, Lagomarsino S. A hysteretic model for “frontal” walls in *Pombalino* buildings. Bulletin of Earthquake Engineering 2012; 10: 1481–1502.

[8] Krawinkler H. Stanford University. Dept. of Civil Engineering, Consortium of Universities for Research in Earthquake Engineering (CUREE). Development of a testing protocol for woodframe structures. CUREE-Caltech Woodframe Project Rep.; 2001.

[9] Ferreira J, Teixeira M, Duţu A, Branco F, Gonçalves A. Experimental Evaluation and Numerical Modelling of Timber-Framed Walls. Exp Tech 2012.

[10] Ahmad N, Ali Q, Umar M. Simplified engineering tools for seismic analysis and design of traditional Dhajji-Dewari structures. Bulletin of Earthquake Engineering 2012;10(5):1503-34.

[11] Cardoso R, Lopes M, Bento R. Seismic evaluation of old masonry buildings. Part I: Method description and application to a case-study. Eng Struct 2005 12;27(14):2024-35.

[12] Vintzileou E, Zagkotsis A, Repapis C, Zeris C. Seismic behaviour of the historical structural system of the island of Lefkada, Greece. Constr Build Mater 2007;21(1):225-36.

[13] Ceccotti A, Faccio P, Nart M, Sandhaas C, Simeone P. Seismic Behaviour of Historic Timber-Frame Buildings in the Italian Dolomites, 15th International Symposium Istanbul and Rize (Turkey). 2006.

[14] Ceccotti A, Karacabeyli E. Validation of seismic design parameters for wood-frame shearwall systems, Canadian Journal of Civil Engineering. 2002;29:484-498.

[15] Filiatrault A, Folz B. Performance-based seismic design of wood framed buildings, J.Struct.Eng. 2002;12839-47.

[16] Kouris LAS, Meireles H, Bento R., Kappos AJ. Simple and complex modelling of timber-framed masonry walls in Pombalino buildings, Bulletin of Earthquake Engineering 2014;[in print]: 1-27.

[17] Galassi S, Ruggieri N, Tempesta G. Seismic Performance Evaluation of Timber-framed Masonry Walls. Experimental Tests and Numerical Modelling, 1st International Symposium on Historic Earthquake - Resistant Timber Frames in the Mediterranean Region, Rende - Cosenza, Italy, 2013.

[18] Kouris LAS, Kappos AJ. Detailed and simplified non-linear models for timber-framed masonry structures. J.Cult.Heritage 2012;13(1):47-58.

[19] Hill R. A Theory of the Yielding and Plastic Flow of Anisotropic Metals. Proceedings of the Royal Society of London. Series A, Mathematical and Physical Sciences 1948;193(1033):281-97.

[20] Shih CF, Lee D. Further developments in anisotropic plasticity. J Eng Mater Technol Trans ASME 1978;100(3):294-302

[21] Moses DM, H.G.L. Prion, Stress and failure analysis of wood composites: a new model, Composites Part B: Engineering 2004;35:251-261.

[22] Patton-Mallory M, S.M. Cramer, F.W. Smith, P.J. Pellicane, Nonlinear material models for analysis of bolted wood connections, Journal of structural engineering New York 1997;123:1063-1070.

[23] Tabiei A, Wu J. Three-dimensional nonlinear orthotropic finite element material model for wood, Composite Structures 2000;50:143-149.

[24] CEN [Comité Européen de Normalisation]. Structural timber - strength classes. EN 338 2009.

[25] Meireles H. Seismic Vulnerability of Pombalino Buildings. PhD Thesis. IST Technical University of Lisbon; 2012.

[26] Apostolopoulos C, Sotiropoulos P. Venetian churches of Lefkada, Greece Construction documentation and seismic behaviour "Virgin Mary of the Strangers". Constr Build Mater 2008;22(4):434-43.

[27] Makarios T, Demosthenous M. Seismic response of traditional buildings of Lefkas Island, Greece. Eng. Struct. 2006;28(2):264-78.

[28] ANSYS User's Manual, Revision 13.0,Swanson Analysis Systems, Inc., Houston, PA. (2011).

[29] Malkus DS, T.J.R. Hughes, Mixed finite element methods — Reduced and selective integration techniques: A unification of concepts, Comput.Methods Appl.Mech.Eng. 1978;15:63-81.

[30] Doudoumis IN. Analytical Modelling of Traditional Composite Timber-Masonry Walls. Advanced Materials Research 2010;133:441-6.

[31] Kouris LAS. Assessment of the seismic behaviour of timber-framed masonry buildings), PhD Thesis. Department of Civil Engineering, Aristotle University of Thessaloniki; 2012 [in Greek], available on http://invenio.lib.auth.gr/record/131198/files/GRI-2013-9972.pdf.

[32] Panagopoulos G, Kappos AJ. Bilinear approximation of force-deformation curves. 16th Hellenic Conference of Reinforced Concrete. Paphos, Cyprus, October 21-23, 2009 [in Greek].

[33] CEN [Comité Européen de Normalisation]. EN 1052: Methods of test for masonry; 2000.

**Table 1. The response and the input parameters of TF walls.**

| | **Response Parameters** $\Omega_i$ | | **Input Parameters** $\Lambda_i$ | |
|---|---|---|---|---|
| | **Symbol** | **Designation** | **Designation** | **Symbol** |
| 1 | $\delta_y$ | Yield displacement | Area of the TF panel | $A = H \times L$ |
| 2 | $\delta_u$ | Maximum (failure) displacement | Ratio of the dimensions of the panel | $R = H / L$ |
| 3 | $V_y$ | Yield shear | Thickness of timber elements | $w$ |
| 4 | $V_u$ | Maximum shear | Depth of timber elements | $d$ |
| 5 | $K_{el}$ | Elastic lateral stiffness | Compressive strength of timber | $f_{c,t}$ |
| 6 | $K_{inel}$ | Post-yield lateral stiffness | Vertical loading | $N = 2P + p \cdot L$ |

**Table 2. Compressive strength parallel to the grain and the corresponding elastic moduli in MPa** [24]**.**

| | **C14** | **C16** | **C18** | **C20** | **C22** | **C24** | **C27** | **C30** | **C35** | **C40** |
|---|---|---|---|---|---|---|---|---|---|---|
| $f_{c,0,k}$ | 16 | 17 | 18 | 19 | 20 | 21 | 22 | 23 | 25 | 26 |
| $E_{0,mean}$ | 7000 | 8000 | 9000 | 9500 | 10000 | 11000 | 11500 | 12000 | 13000 | 14000 |

**Table 3. Characteristics of the panels in IST specimens [6] SC2 and SC3.**

| **H** | **L** | **H/L** | **A** | **w*** | **d** | **$f_{ct}$** |
|---|---|---|---|---|---|---|
| [m] | [m] | | [$m^2$] | [m] | [m] | [MPa] |
| 1.3 | 1.32 | 0.98 | 1.72 | 0.10 | 0.1 | 25 |

**Table 4. Application of the empirical expressions to IST specimens.**

| **i** | **$\phi_{,i}$** | **$\lambda_{A,i}$** | **$\lambda_{R,i}$** | **$\lambda_{W,i}$** | **$\lambda_{d,i}$** | **$\lambda_{N,i}$** |
|---|---|---|---|---|---|---|
| $V_y$ | 24.90 | 0.97 | 1.18 | 0.67 | 1 | 1 |
| $V_u$ | 32.90 | 0.94 | 1.19 | 0.67 | 1 | 1 |
| $\delta_y$ | 0.78 | - | 0.88 | - | 1 | 1 |
| $\delta_u$ | 6.08 | 0.90 | - | - | 1 | 1 |

**Table 5. Comparison of LNEC experimental results with those of the macro-model.**

| | max shear | | difference | max displacement | | difference |
|---|---|---|---|---|---|---|
| | (kN) | | (%) | (cm) | | (%) |
| G1 | 71.6 | -60.6 | 12% | 12.5 | -10.3 | -21% |
| model | 58.8 | | | 14.49 | | |
| G2 | 71.0 | -63.4 | 6% | 12.3 | -9.9 | -7% |
| model | 63.4 | | | 12 | | |
| G3 | 46.8 | -59.2 | 5% | 11.8 | -11.4 | -3% |
| model | 50.4 | | | 12.0 | | |


**Figure 1. TF panel with two diagonal braces subjected to a horizontal force.**

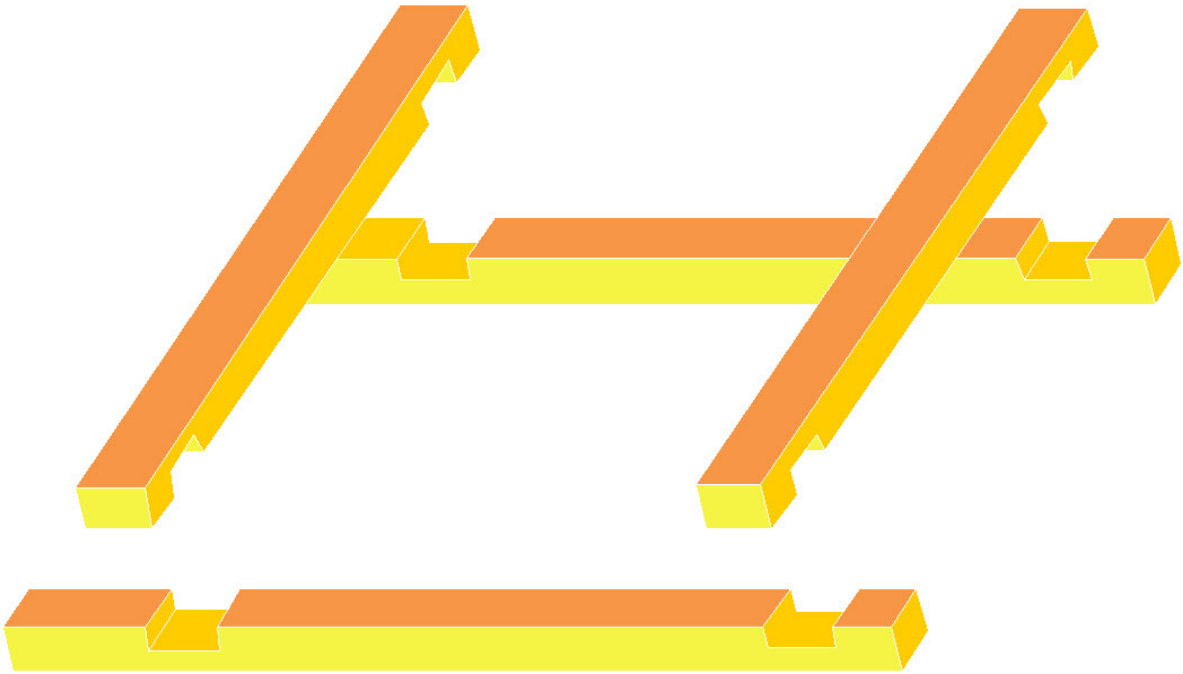

(a)

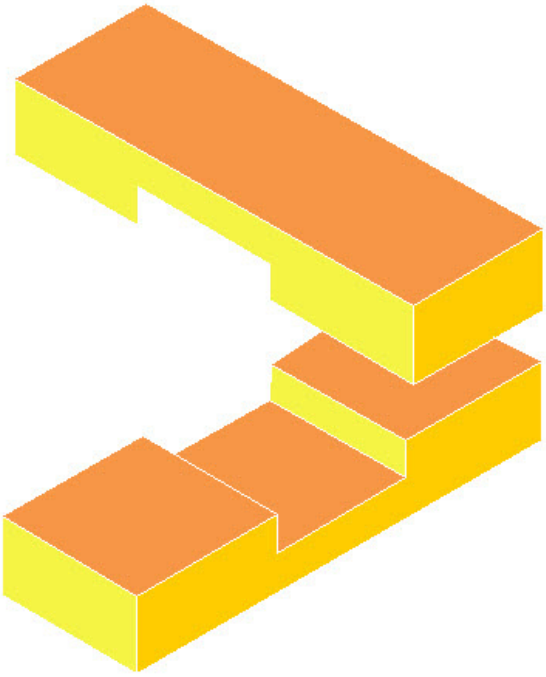

(b)

**Figure 2. T-shaped lap joint for timber connections between: (a) beams and posts and (b) diagonals.**

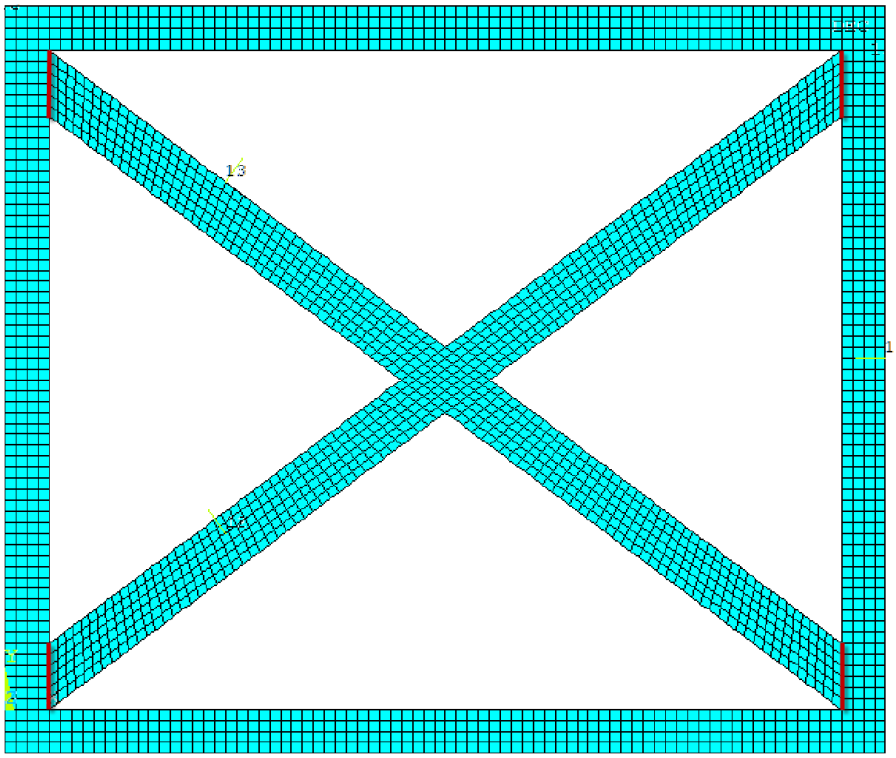

(a)

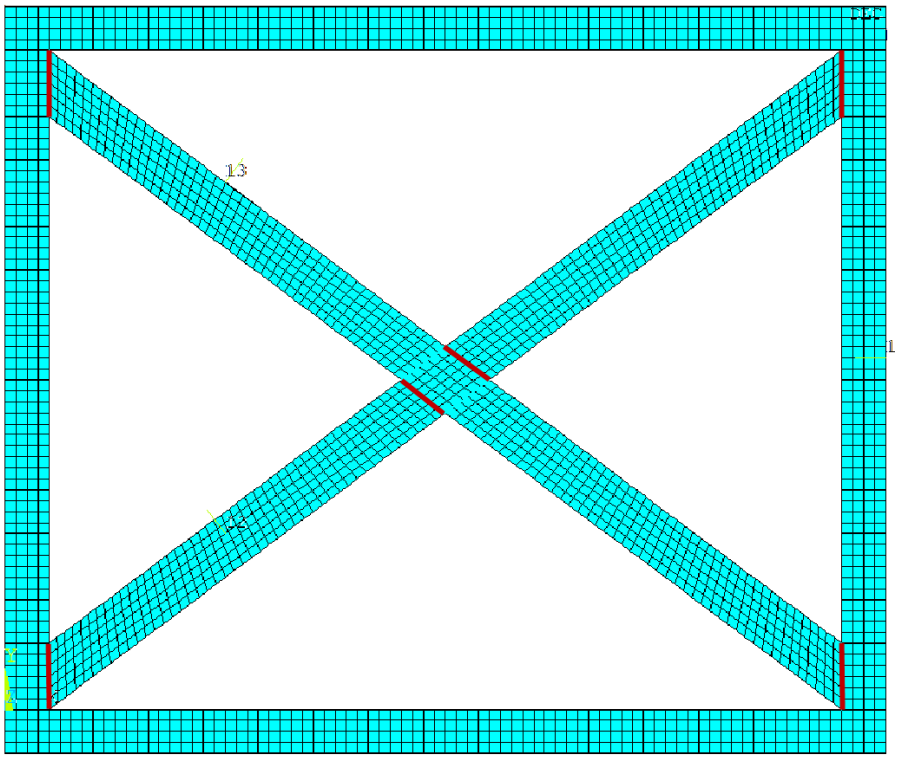

(b)

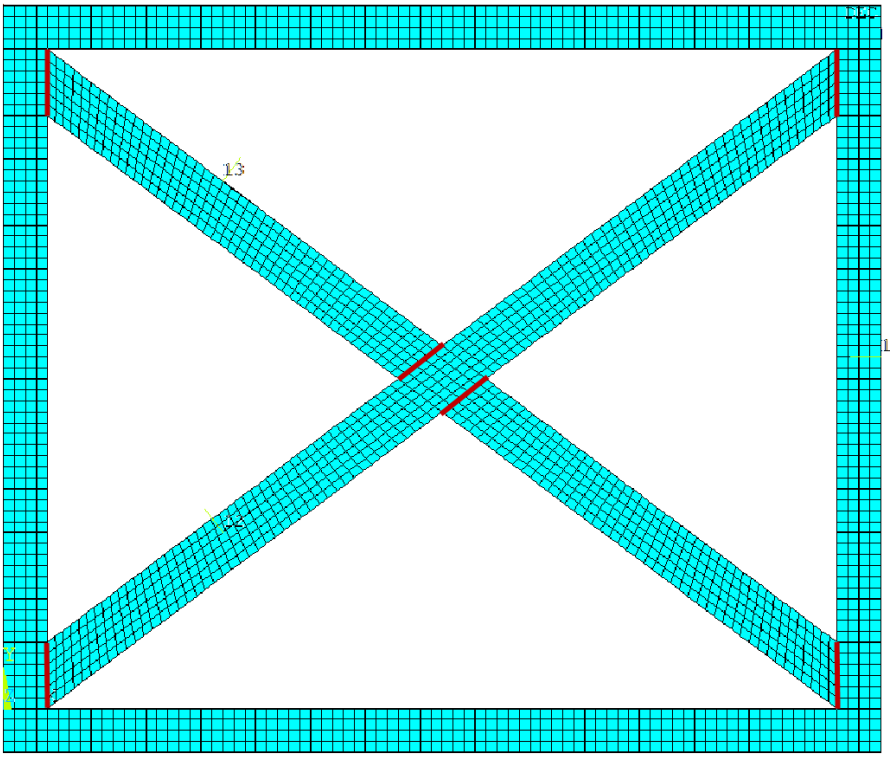

(c)

**Figure 3. Examined configurations of the diagonals joints (in thick red line the discontinuities): (a) rigid connection between the diagonals, (b) continuous diagonal in compression and two-segment diagonal in tension and (c) continuous diagonal in tension and two-segment diagonal in compression.**

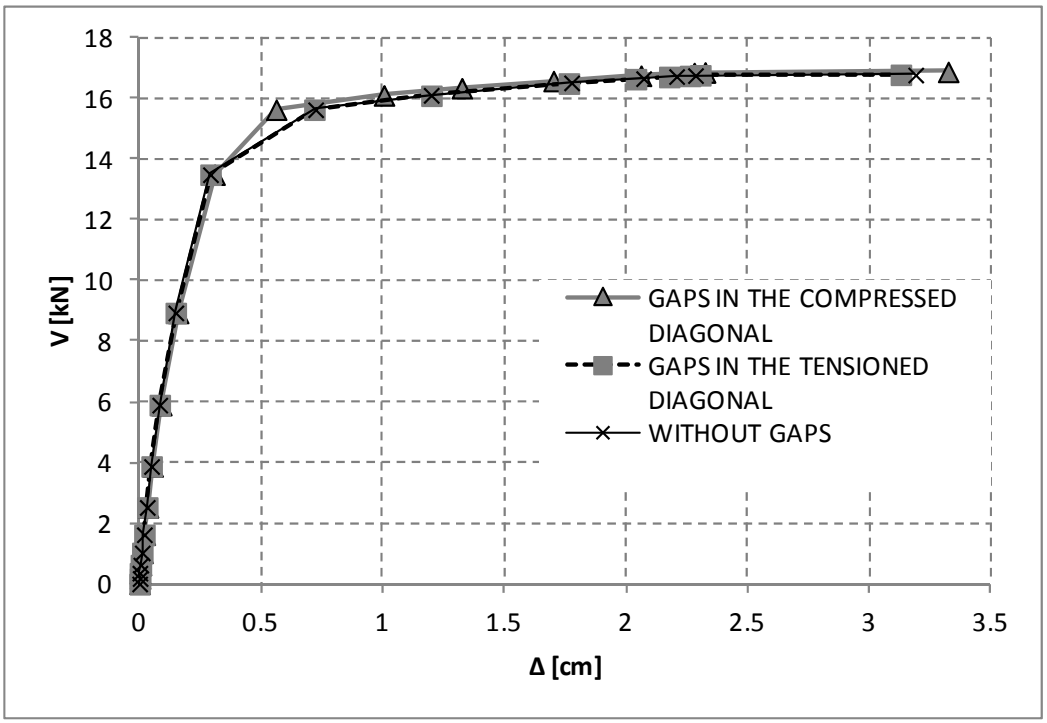


**Figure 4. Capacity curves for a TF panel with three different types of connections between its diagonals.**

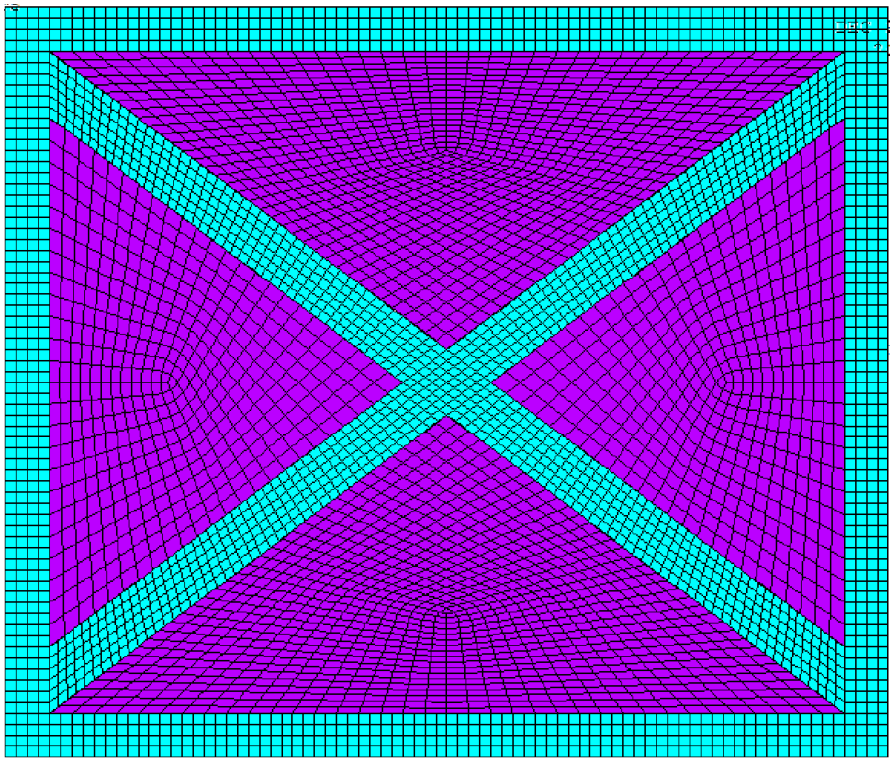

(a)

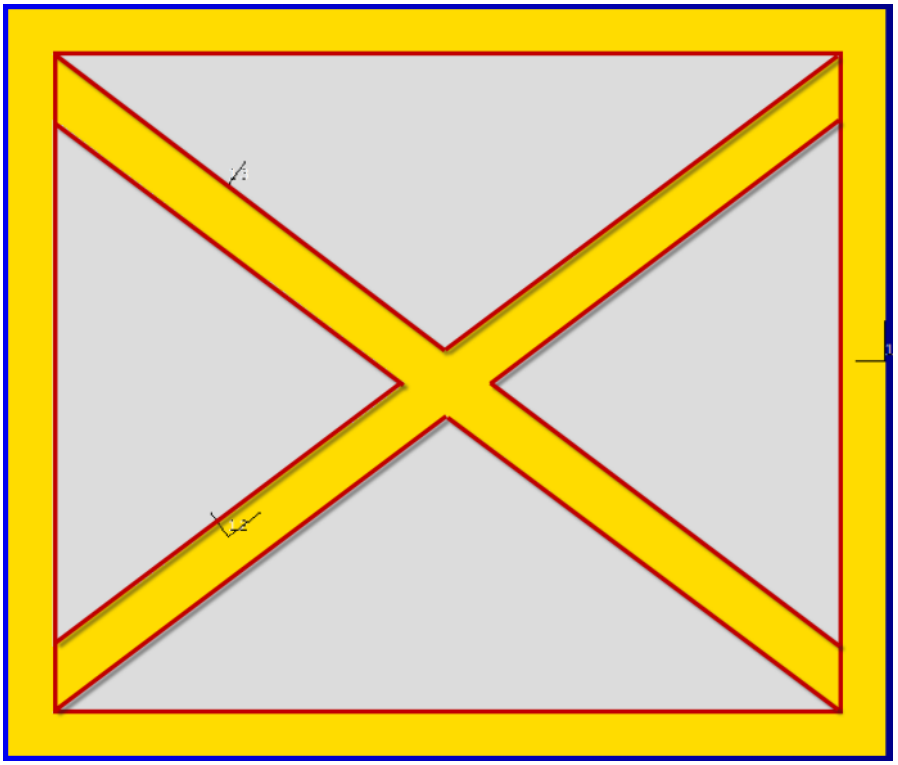

(b)

**Figure 5. TF panel with masonry infills: (a) simulation with FE (in light blue timber elements and in magenta masonry elements) and (b) the contact surfaces in solid red lines.**

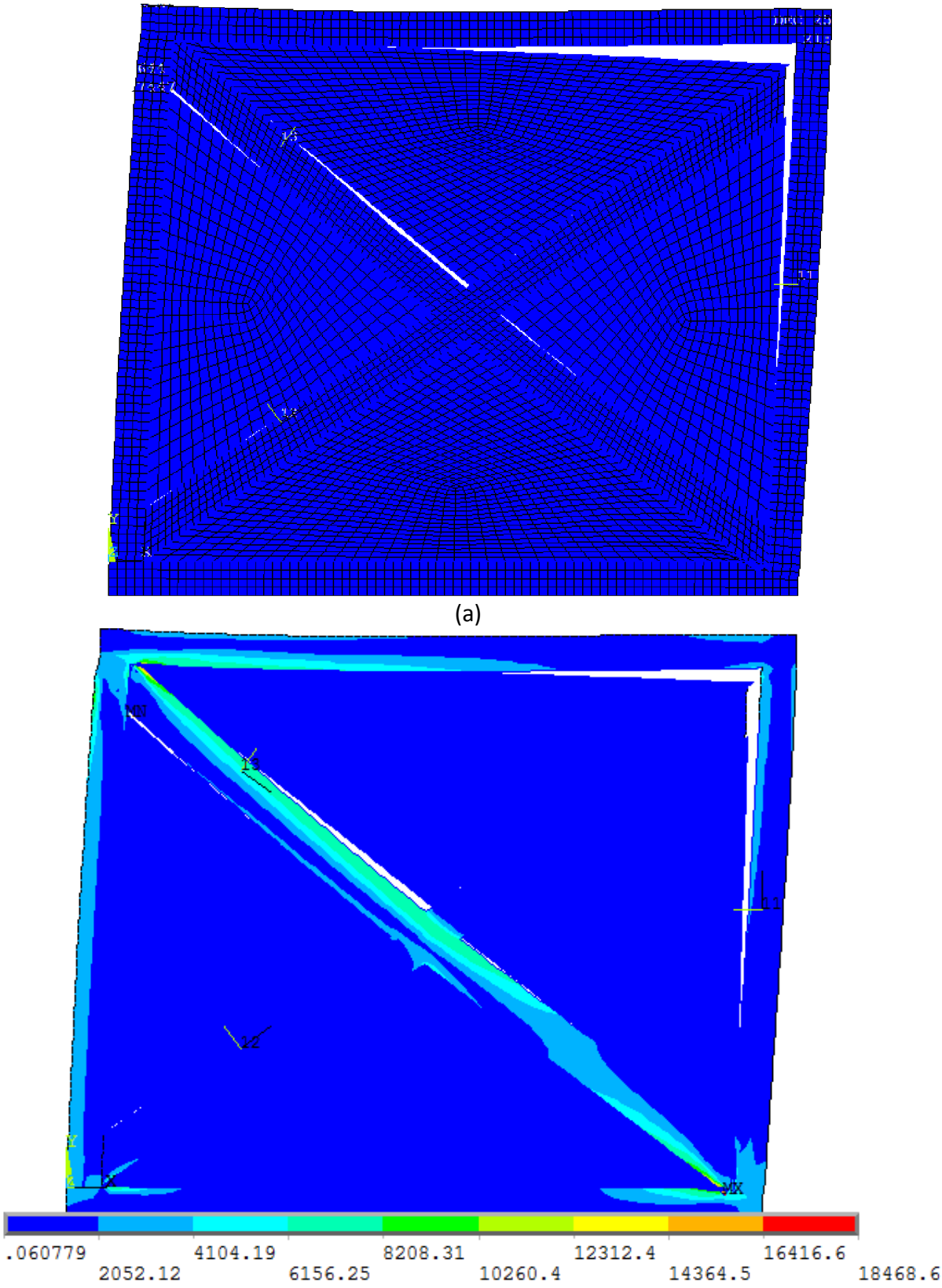


**Figure 6. Horizontally loaded TF walls: (a) deformed shape and (b) stresses (in kPa) immediately prior to the final step of the pushover analysis.**

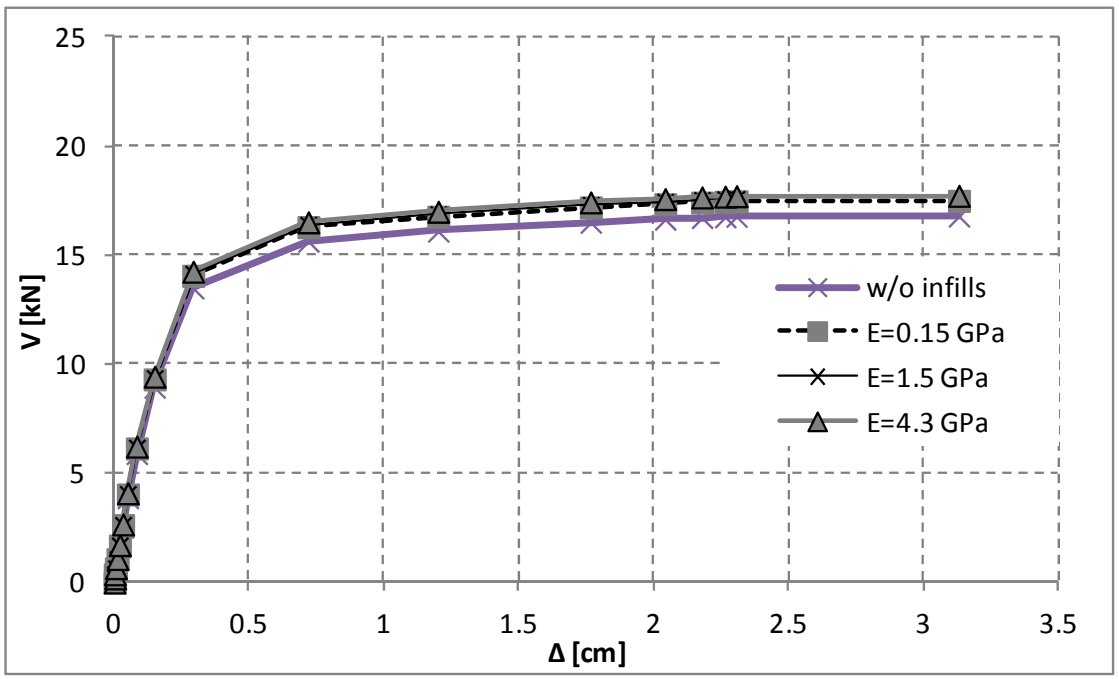


**Figure 7. Pushover curves of the TF panels with different modulus of elasticity of their masonry infills.**

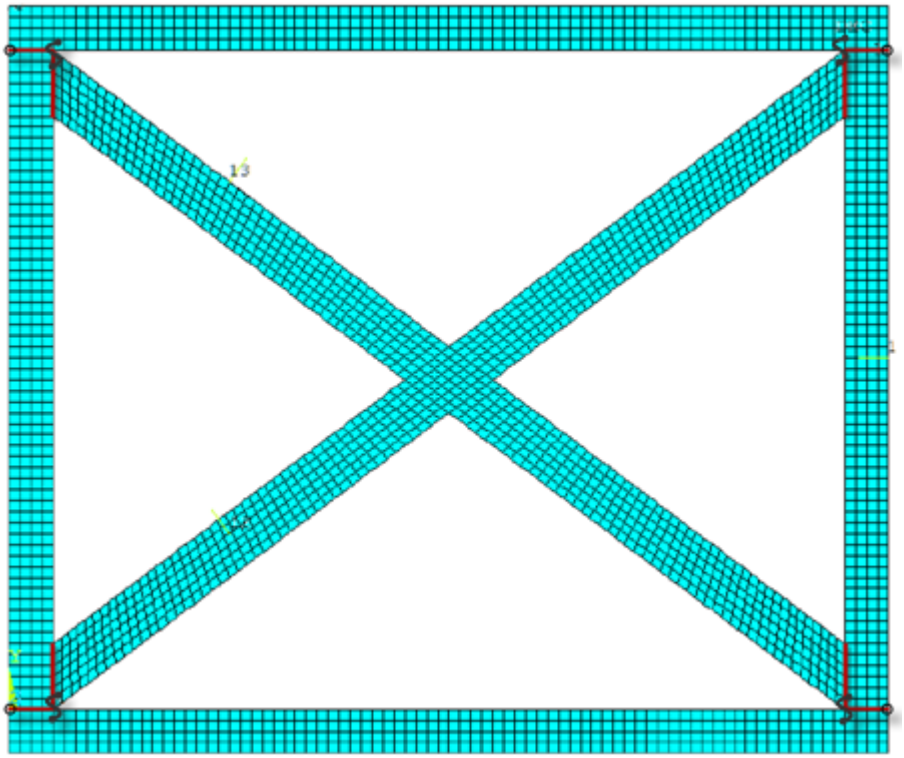

(a)

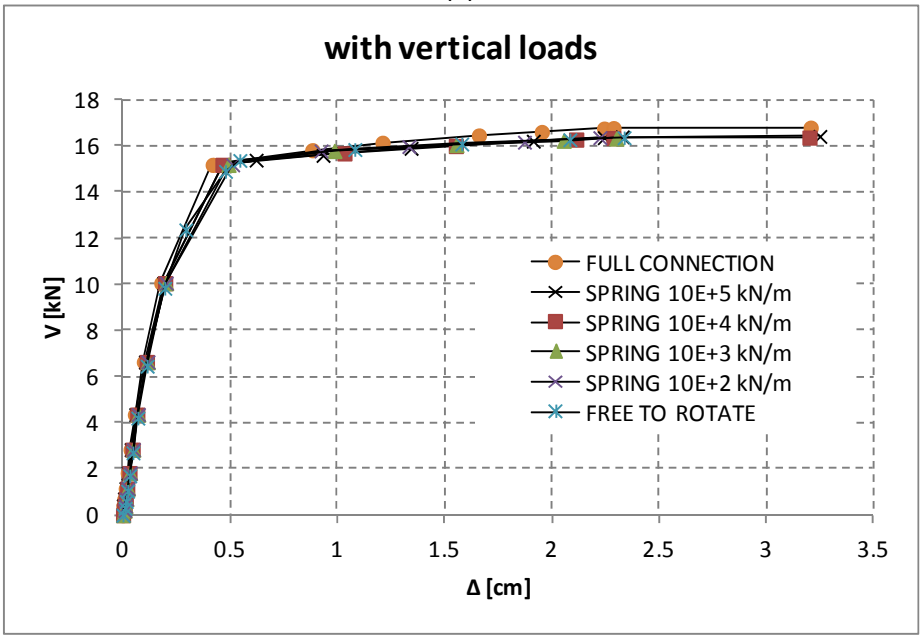
with vertical loads
V [kN]
Δ [cm]
0
2
4
6
8
10
12
14
16
18
0
0.5
1
1.5
2
2.5
3
3.5
FULL CONNECTION
SPRING 10E+5 kN/m
SPRING 10E+4 kN/m
SPRING 10E+3 kN/m
SPRING 10E+2 kN/m
FREE TO ROTATE

(b)

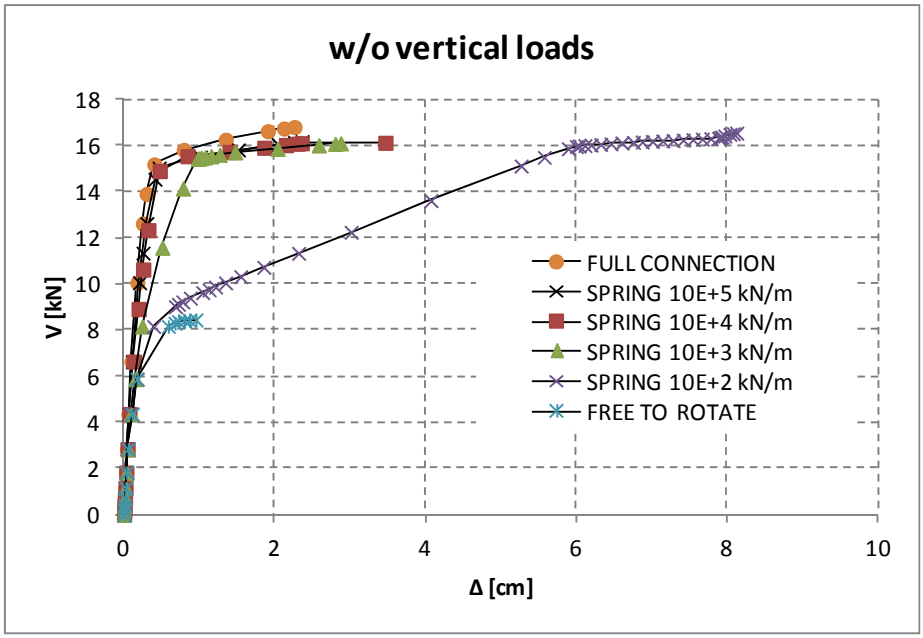


(c)

**Figure 8. TF panel with gap between beams and post: (a) model configuration, wherein the red solid lines denote the gaps, the black circles the potential center of rotation and the black splines the (zero length) springs, pushover curves (shear force vs. top displacement) for various stiffnesses of the springs when (b) the frame vertically loaded, and (c) vertically unloaded.**

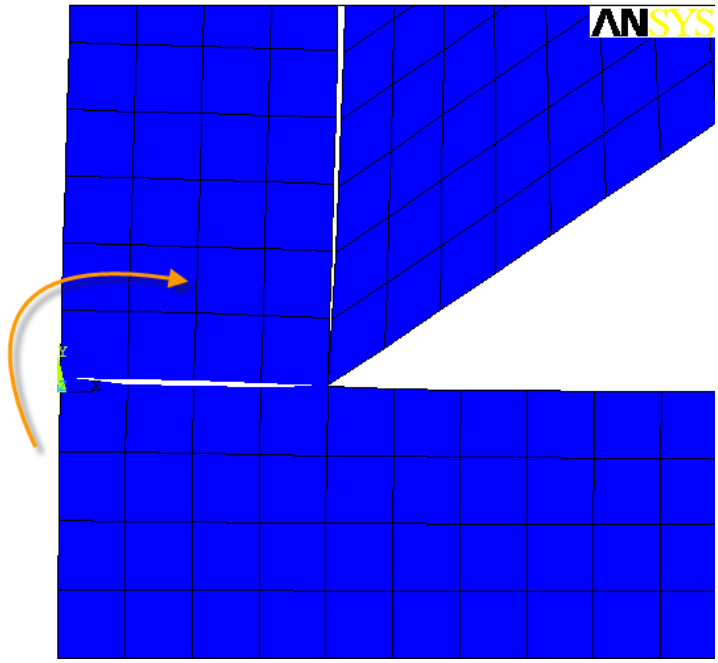


**Figure 9. Rotation about the spring rather than the node.**

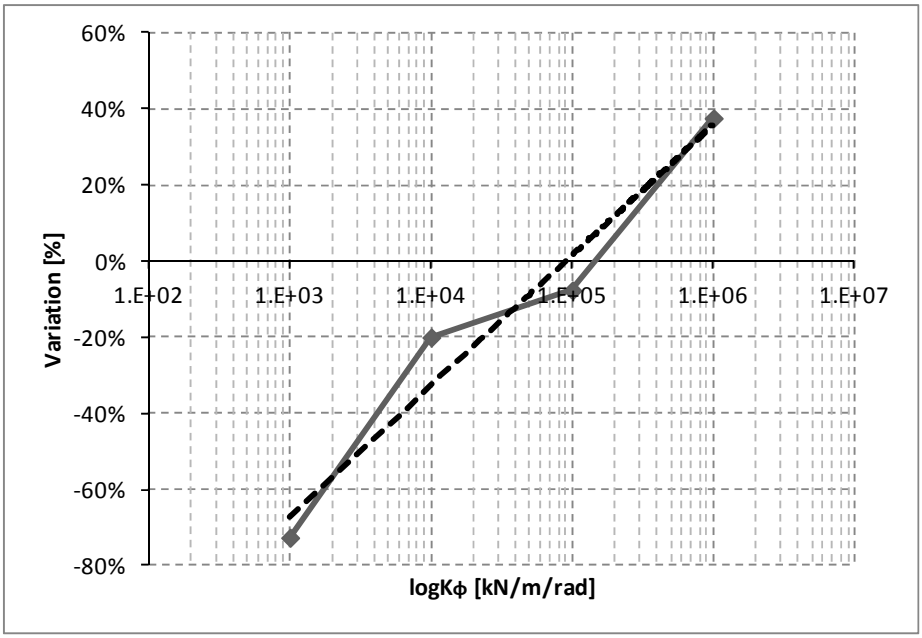


**Figure 10. Variation of the maximum displacement with the rotational spring stiffness in logarithmic scale.**

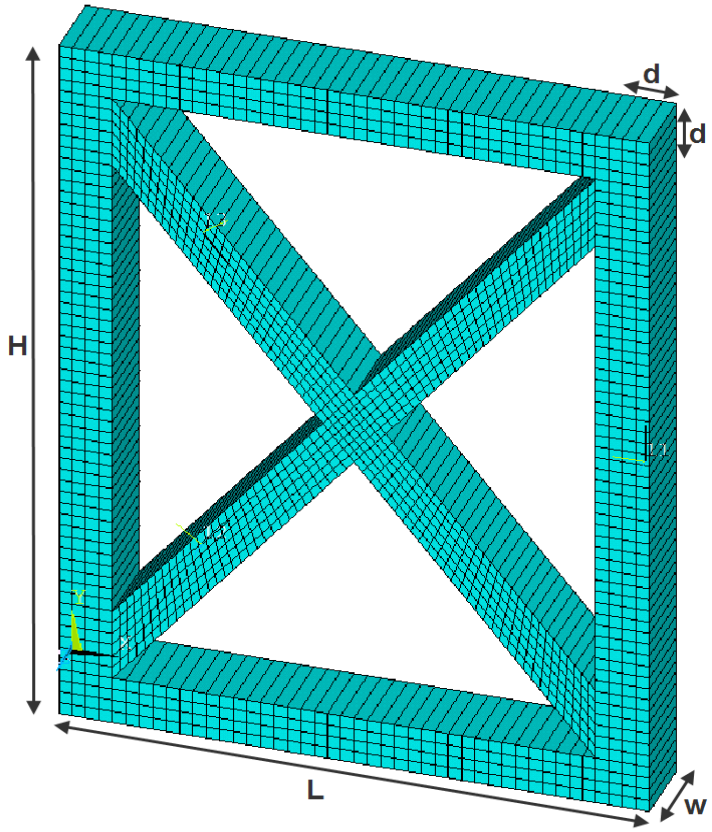


**Figure 11. Geometry of the reference TF panel.**

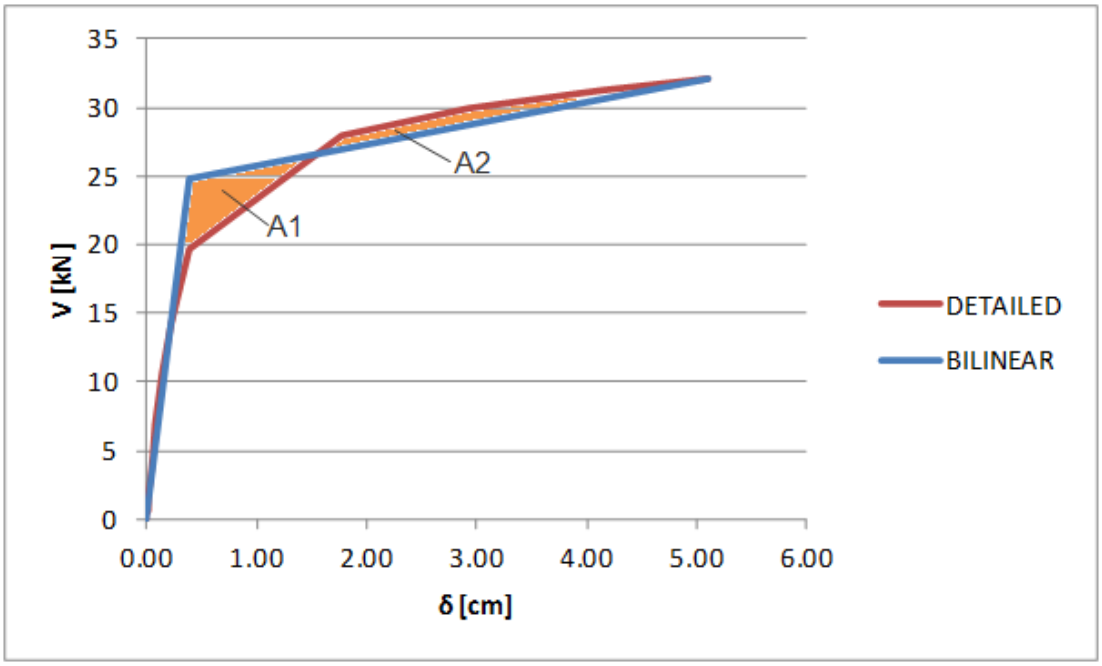


**Figure 12. Bilinearization of the pushover curve by equating the areas between the two curves.**

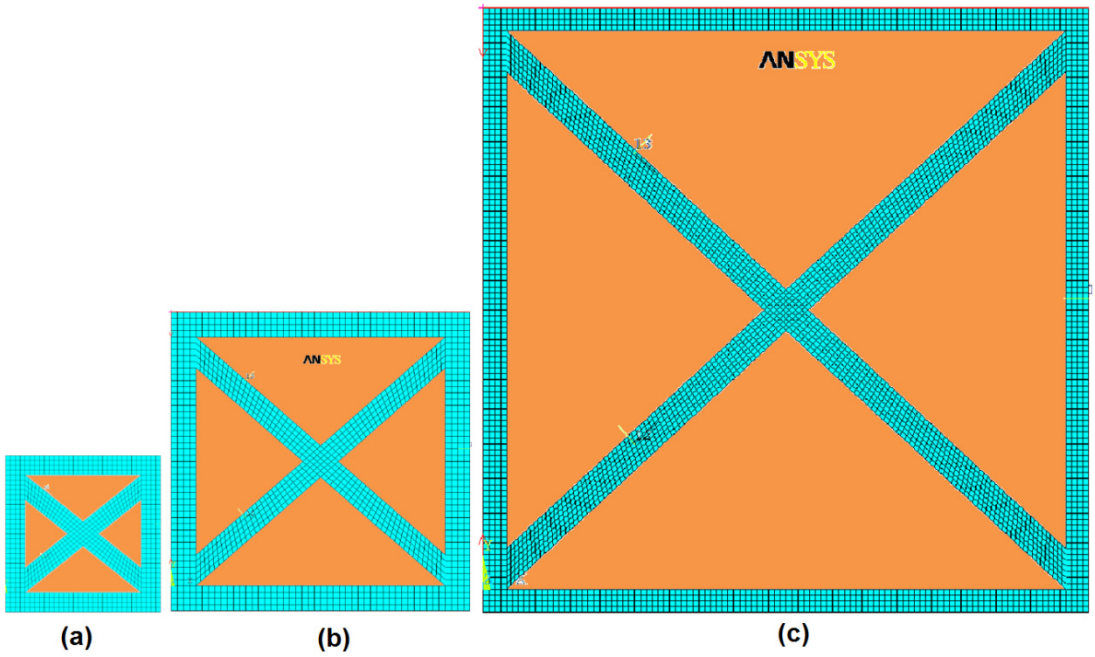


**Figure 13. Sketch of three panels used in the parametric analysis of *A*: (a) min area (0.6×0.6m$^2$), (b) intermediate area (1.2×1.2m$^2$) and (c) max area (2.4×2.4m$^2$).**

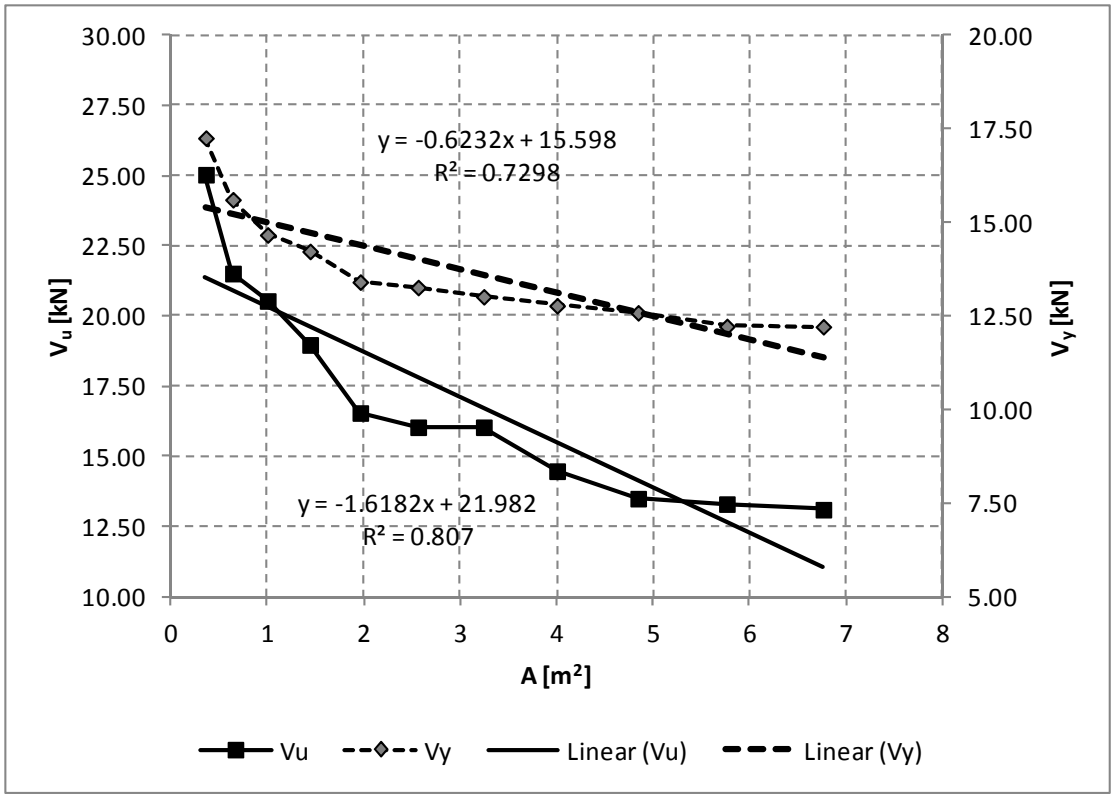
30.00
27.50
25.00
22.50
20.00
17.50
15.00
12.50
10.00
20.00
17.50
15.00
12.50
10.00
7.50
5.00
0
1
2
3
4
5
6
7
8
y = -0.6232x + 15.598
R² = 0.7298
y = -1.6182x + 21.982
R² = 0.807
Vu [kN]
Vy [kN]
A [m²]
Vu
Vy
Linear (Vu)
Linear (Vy)

(a)

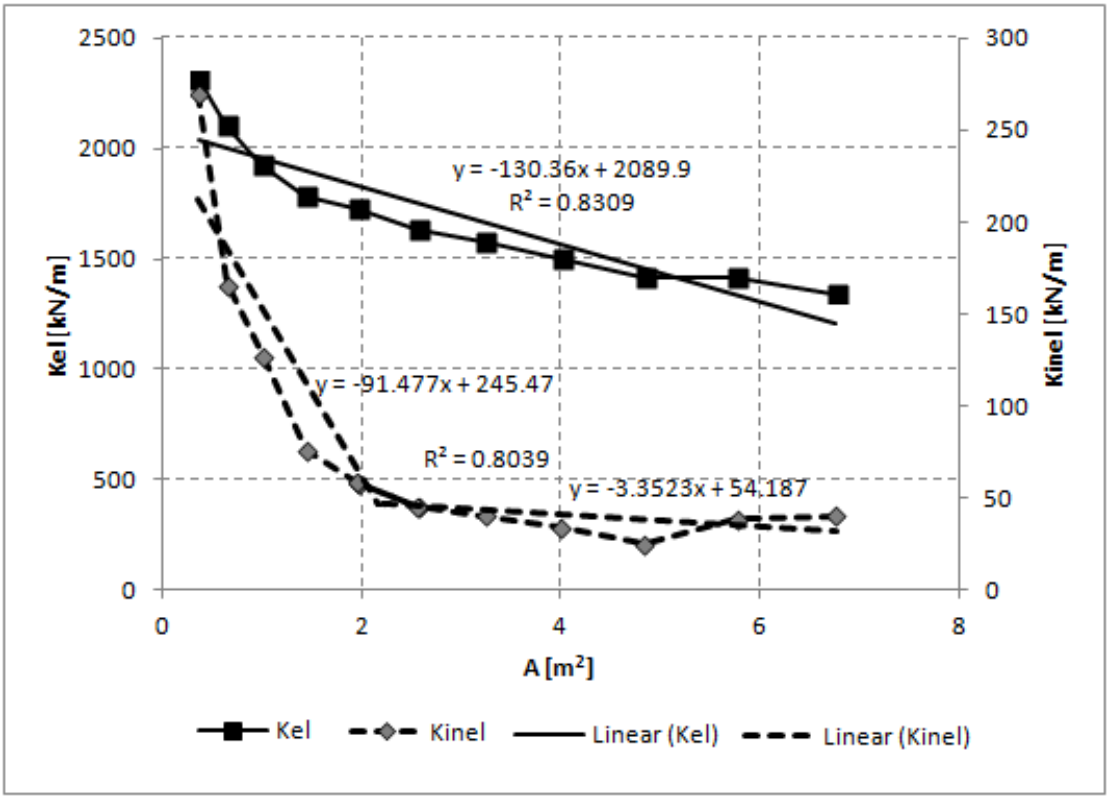
2500
2000
1500
1000
500
0
300
250
200
150
100
50
0
0
2
4
6
8
y = -130.36x + 2089.9
R² = 0.8309
y = -91.477x + 245.47
R² = 0.8039
y = -3.3523x + 54.187
Kel [kN/m]
Kinel [kN/m]
A [m²]
Kel
Kinel
Linear (Kel)
Linear (Kinel)

(b)

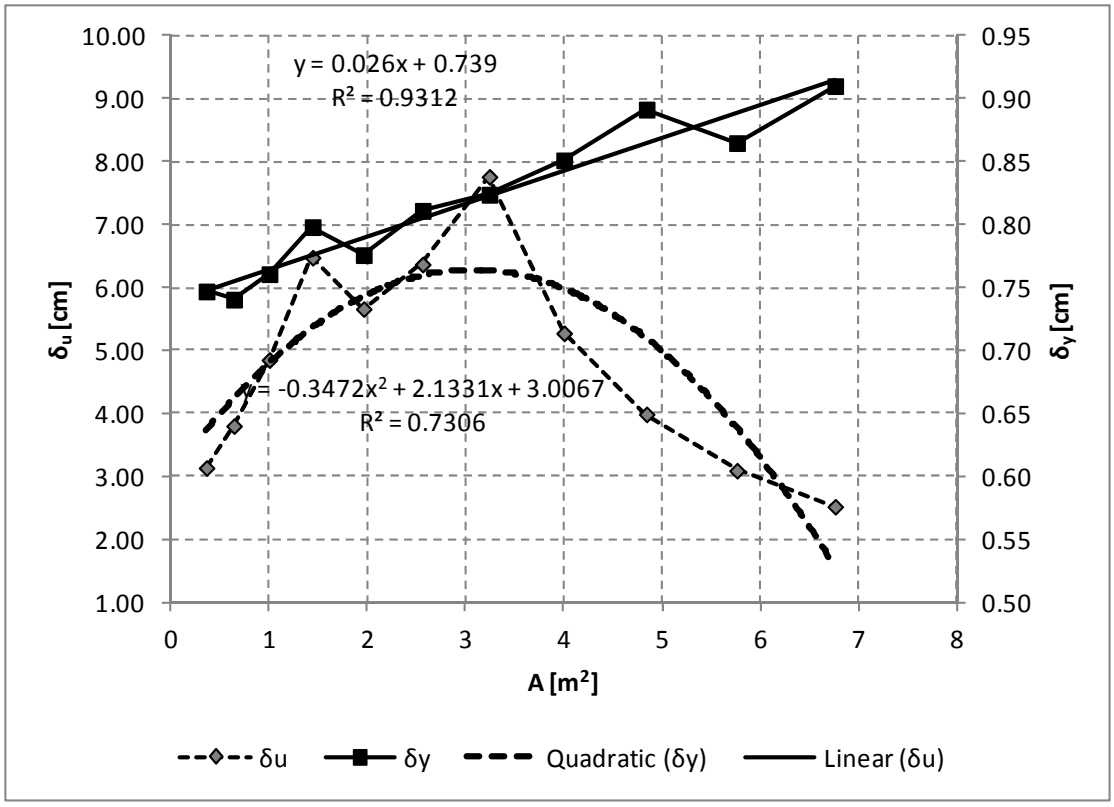


(c)

**Figure 14. Variation with *A* of: (a) lateral strength, (b) lateral stiffnesses and (c) displacements at yielding and failure.**

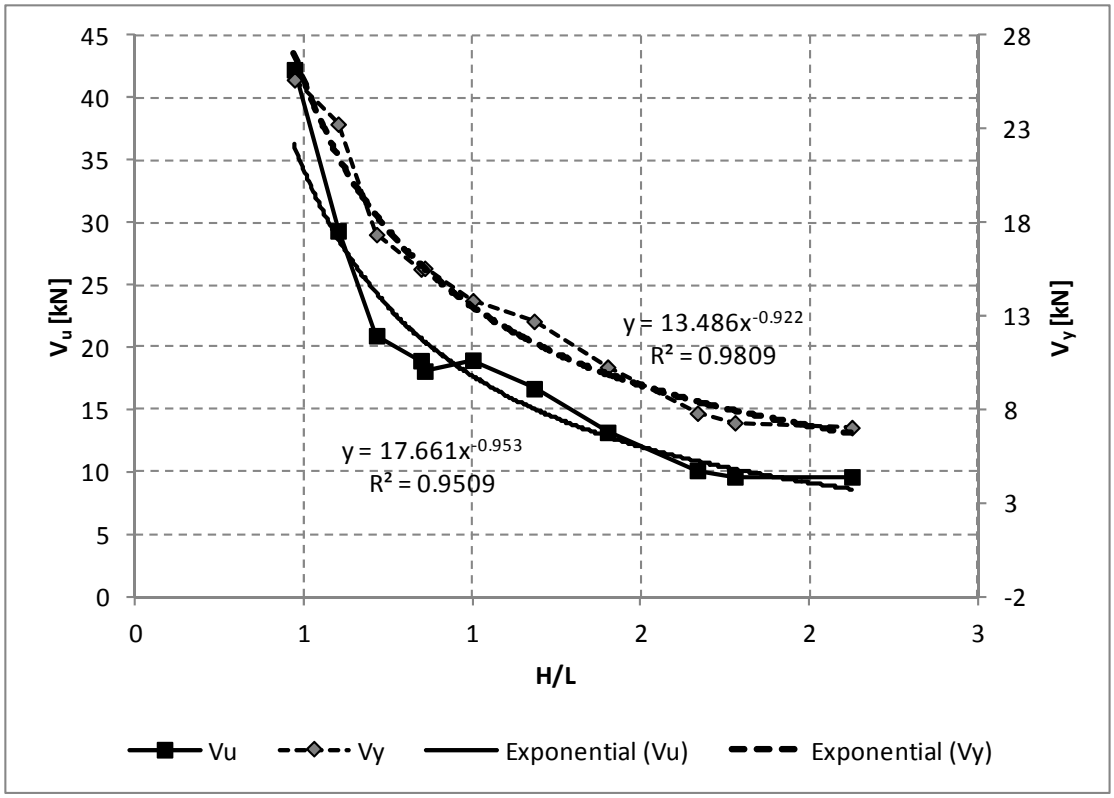


**Figure 15. Variation of shears at yielding $V_y$ and failure $V_u$ with *H/L.***

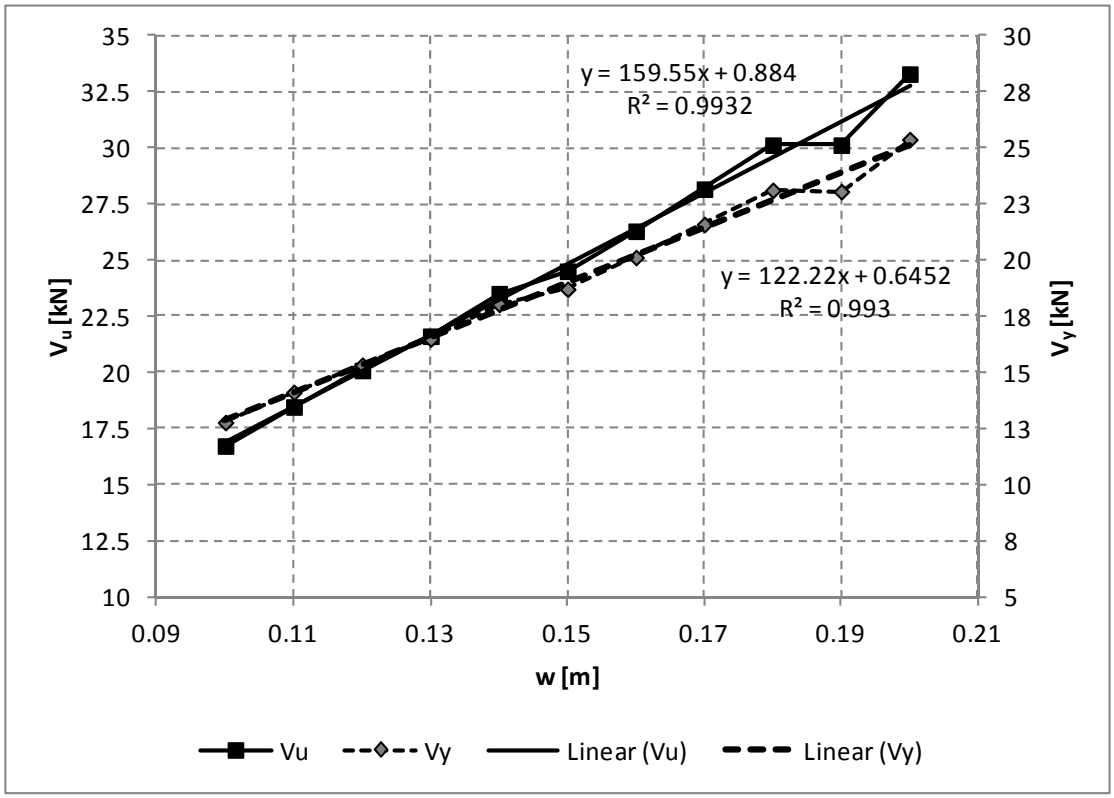


**Figure 16. Variation of shear at yielding $V_y$ and failure $V_u$ with *w.***

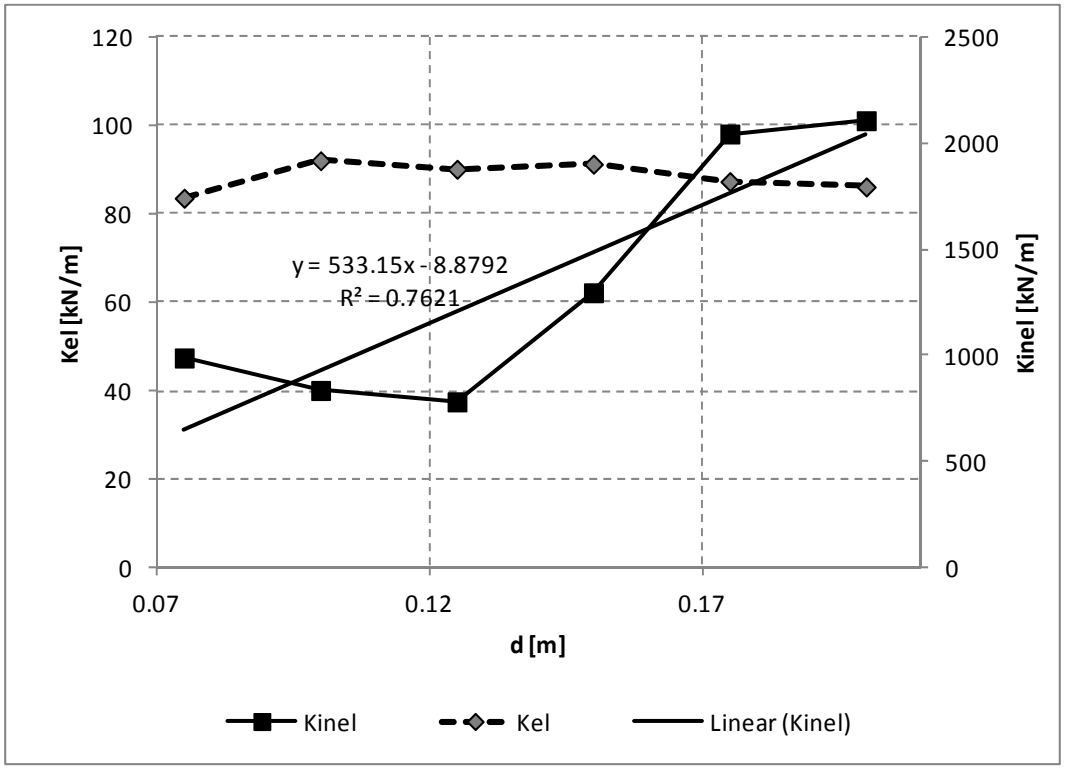


**Figure 17. Variation of elastic and post-elastic lateral stiffnesses with depth *d*.**

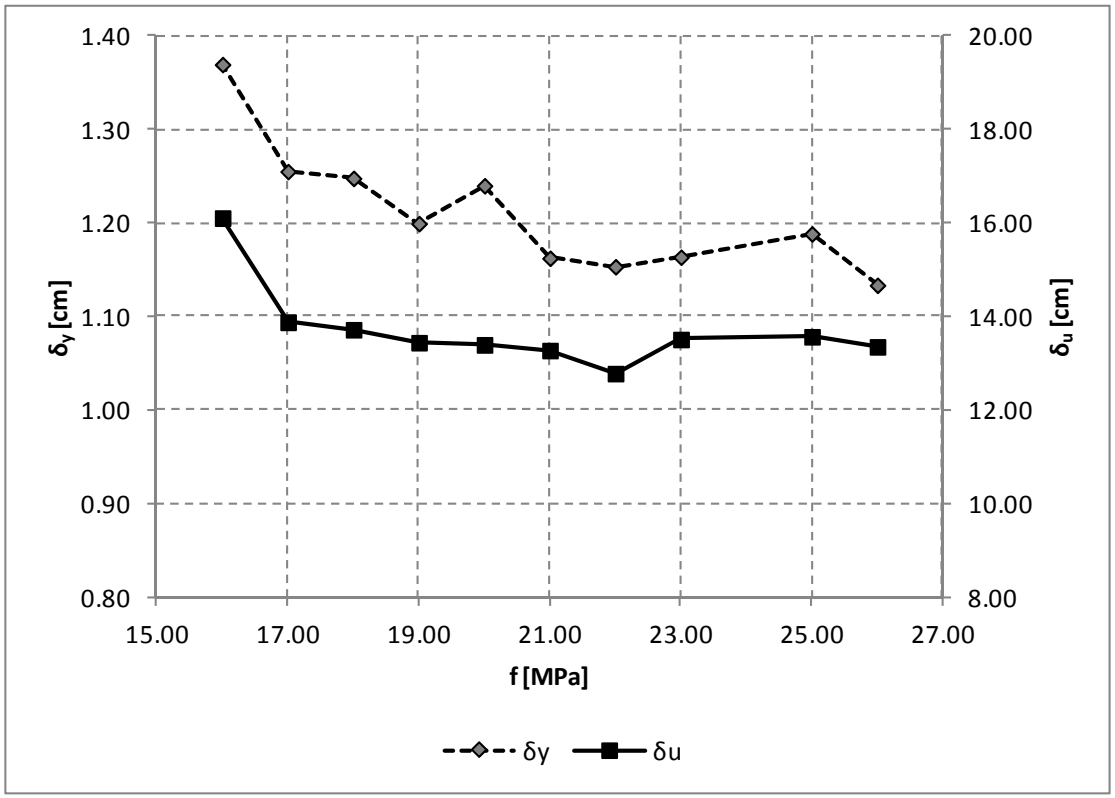


**Figure 18. Variation of displacements $\delta_y$ and $\delta_u$ with timber strength $f_{c,t}$.**

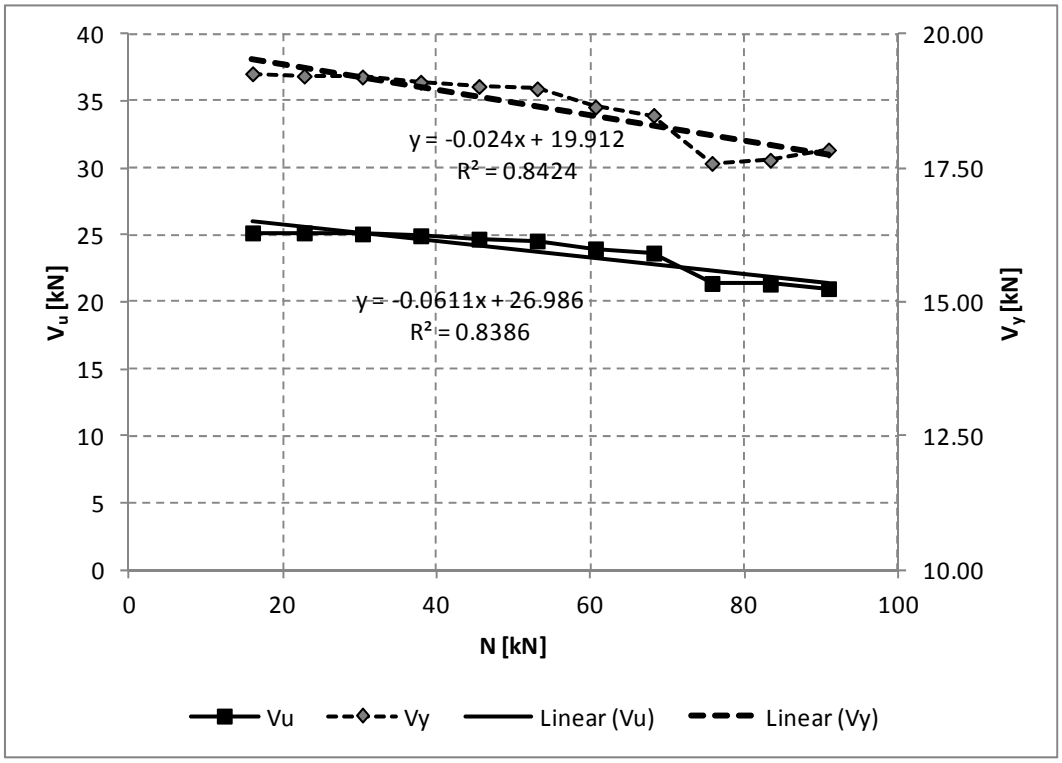
y = -0.024x + 19.912
R² = 0.8424
y = -0.0611x + 26.986
R² = 0.8386
Vu [kN]
Vy [kN]
N [kN]
Vu
Vy
Linear (Vu)
Linear (Vy)

(a)

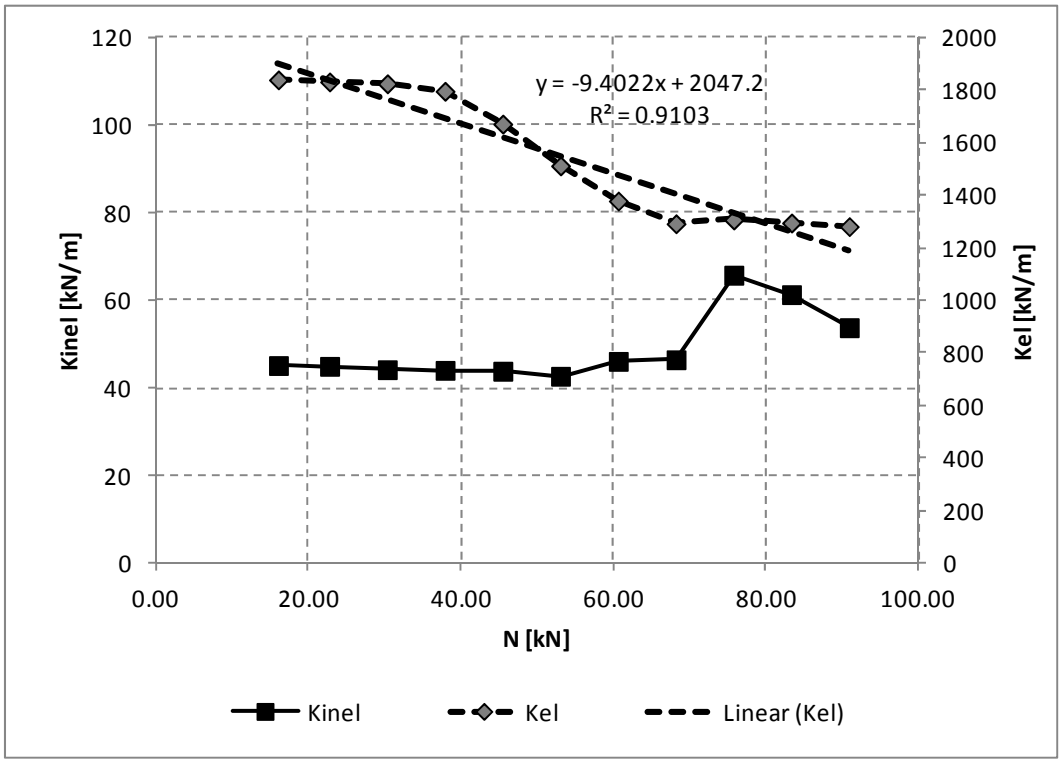
y = -9.4022x + 2047.2
R² = 0.9103
Kinel [kN/m]
Kel [kN/m]
N [kN]
Kinel
Kel
Linear (Kel)

(b)

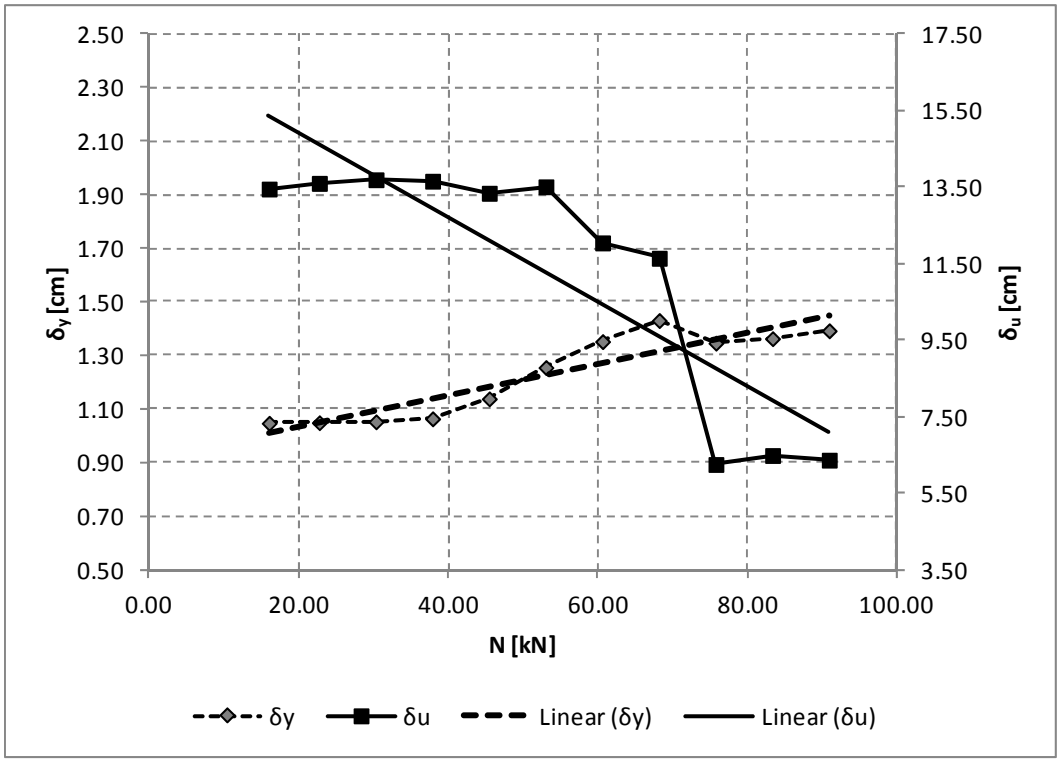


(c)

**Figure 19. Variation with *N* of: (a) shear strength, (b) lateral stiffness, and (c) displacements at yielding and failure.**

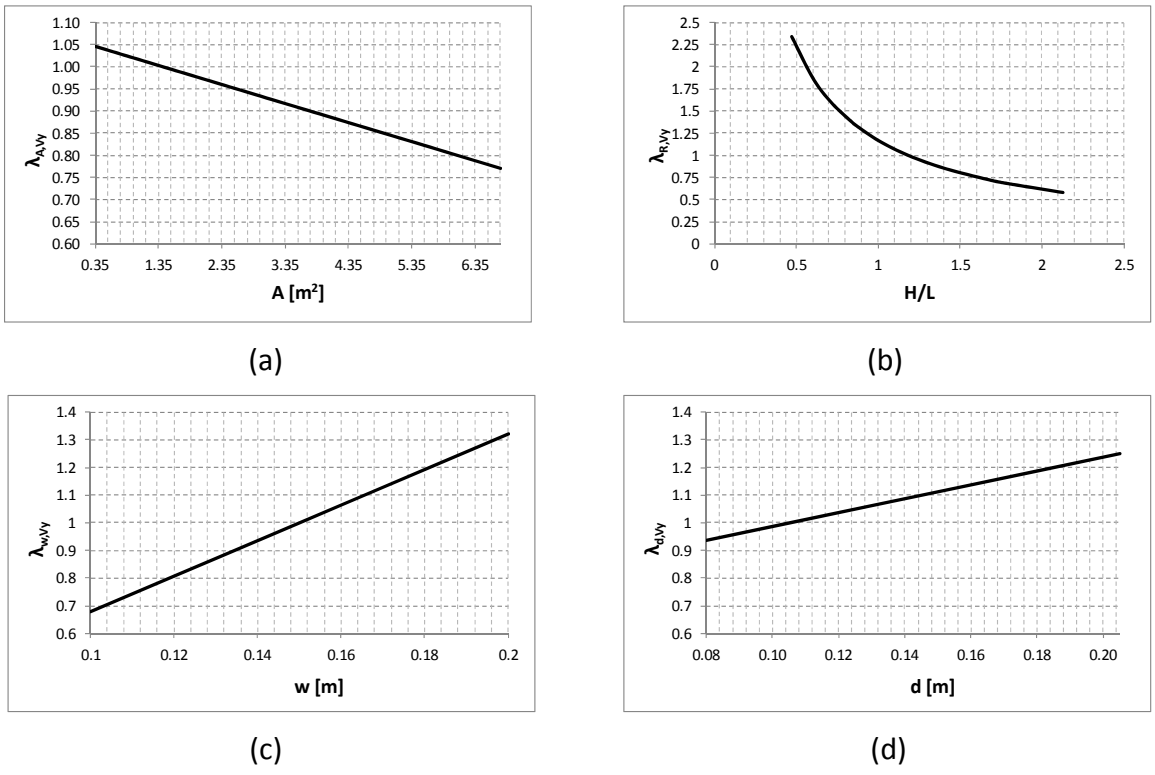


**Figure 20. Correction coefficients for shear at yielding $V_y$.**

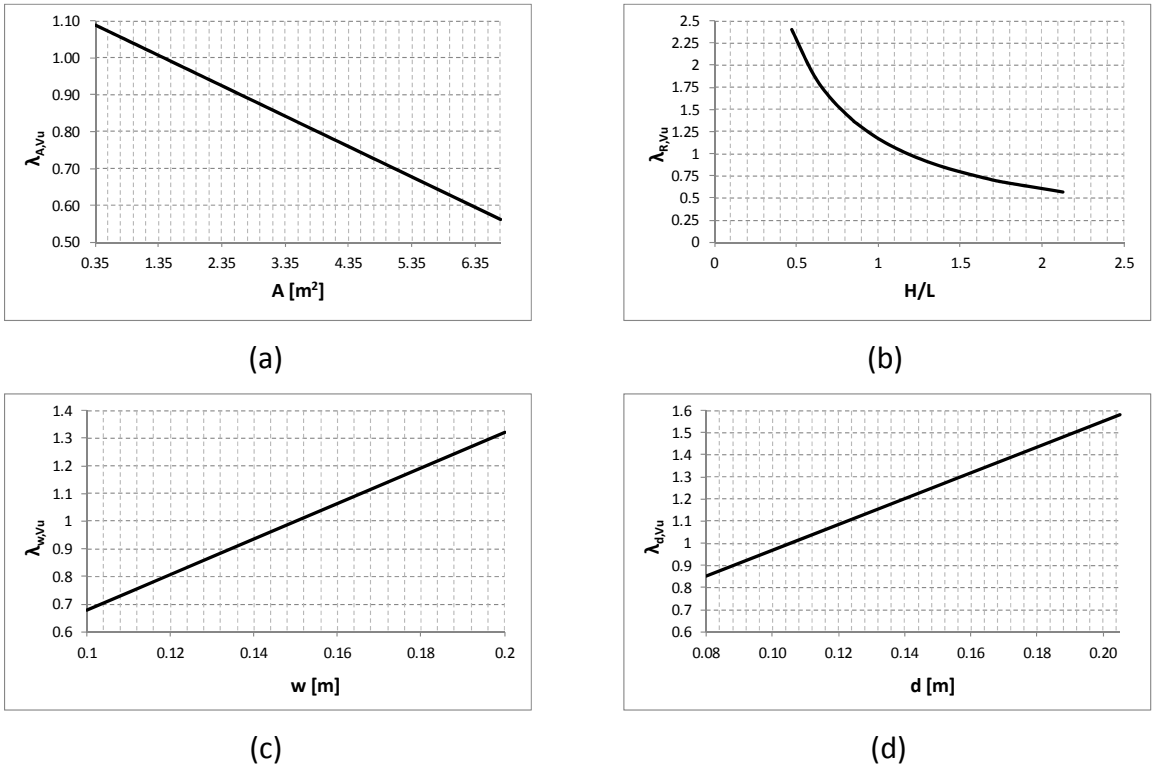


**Figure 21. Correction coefficients for maximum shear $V_u$.**


**Figure 22. Correction coefficient for yield displacement $\delta_y$.**

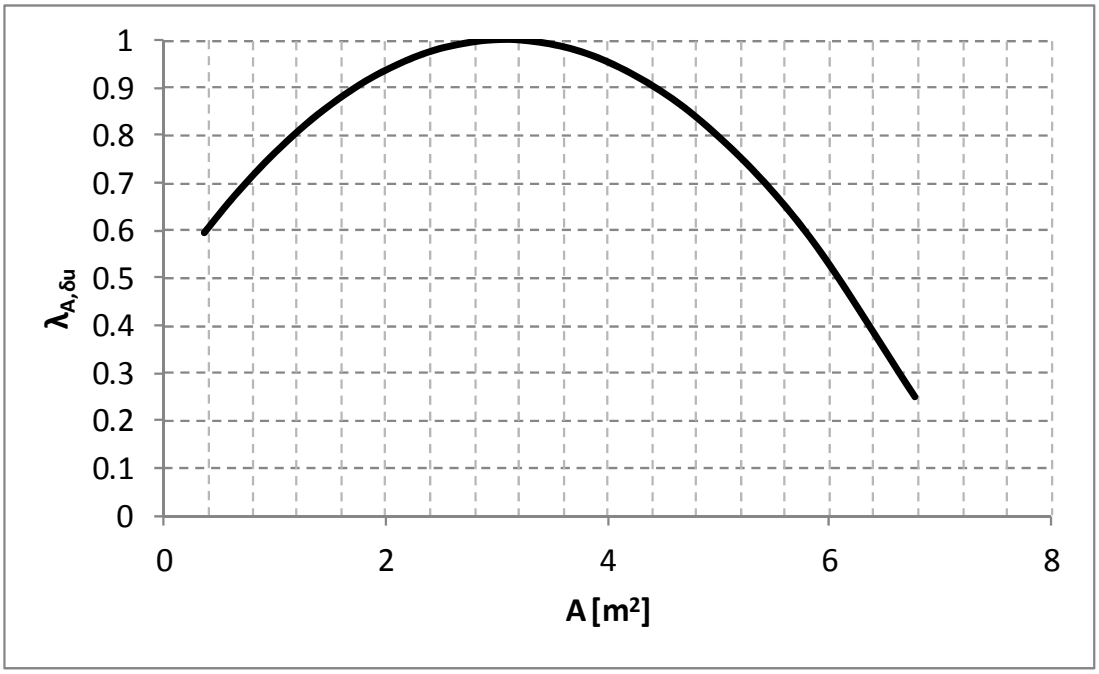


**Figure 23. Correction coefficient for maximum displacement $\delta_u$.**

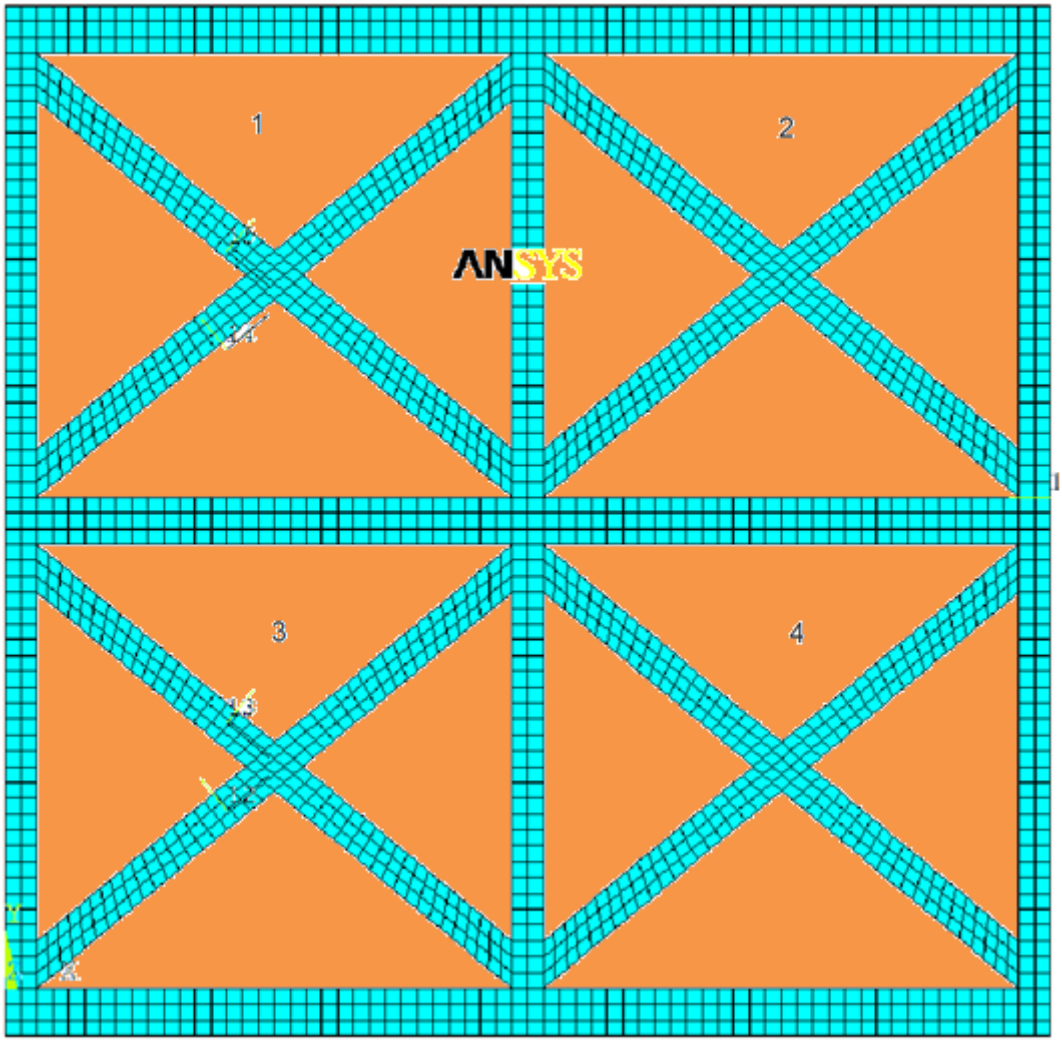


(a)

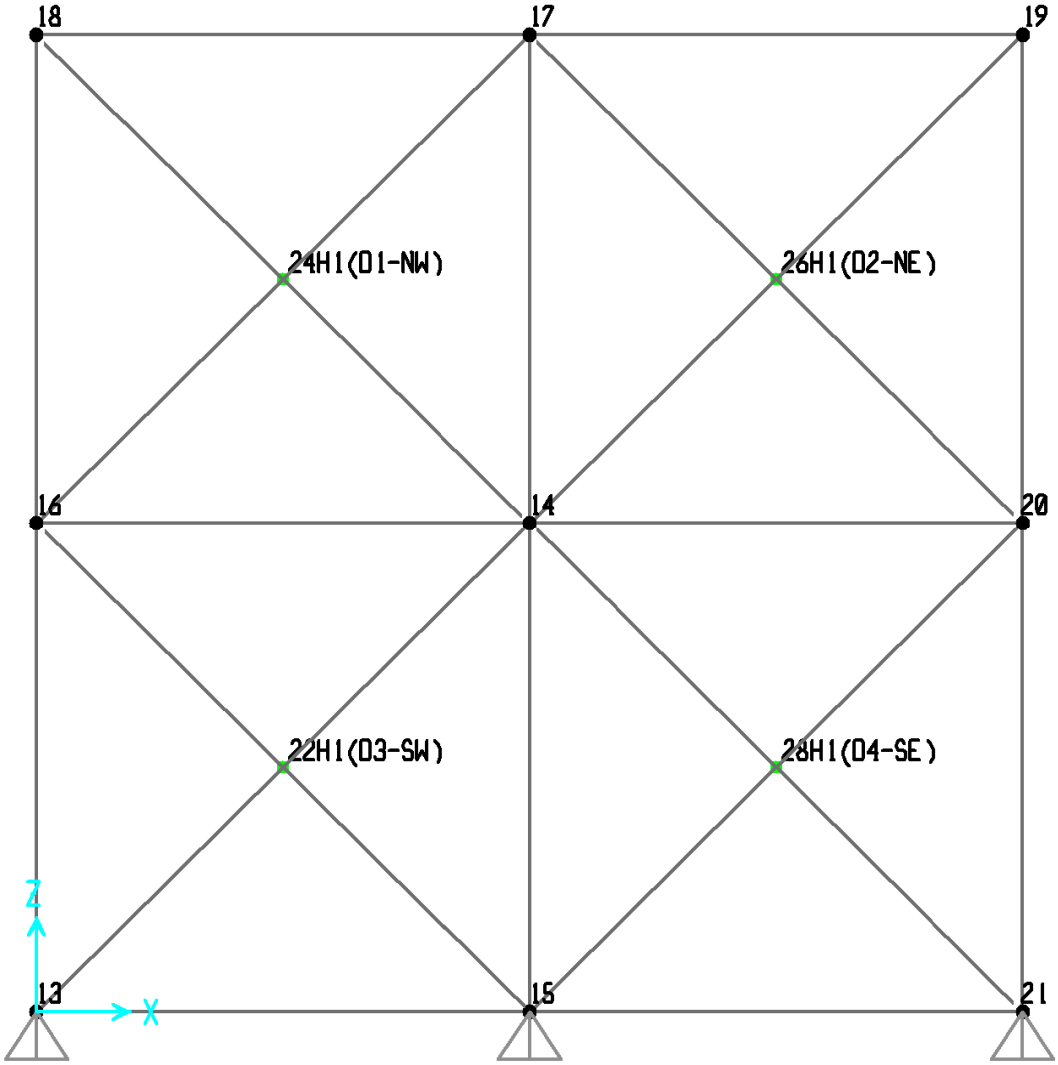


(b)

**Figure 24. (a) Finite element discretization and (b) macro-modelling of SC1 and SC2 specimens.**

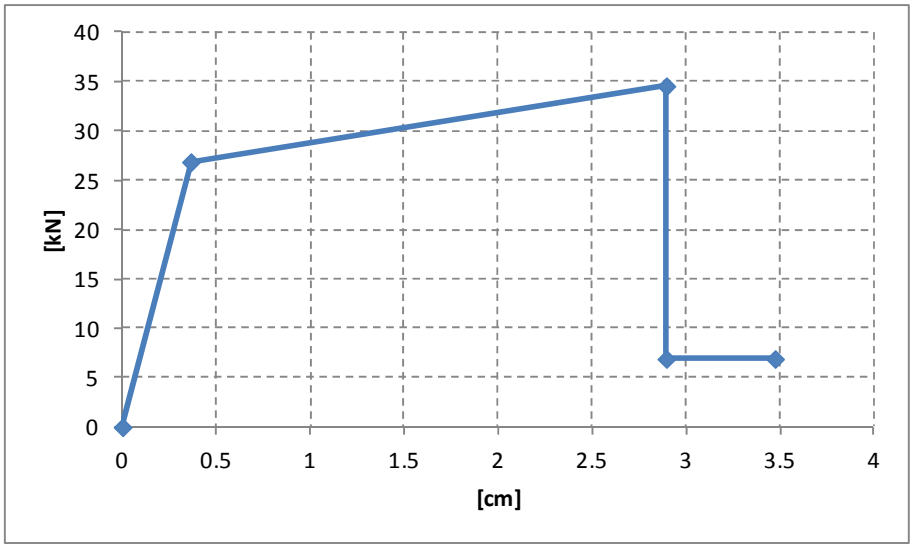


**Figure 25. The axial plastic hinge of the diagonals.**

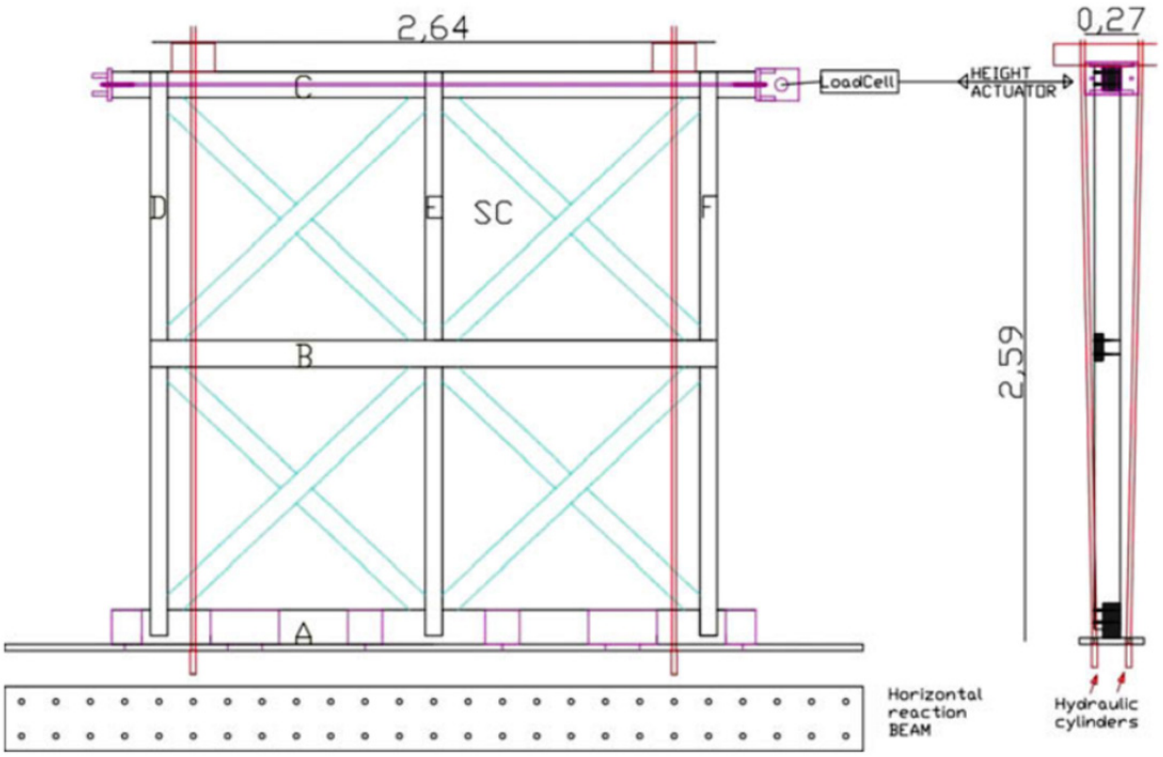
2,64
0,27
C
D
E
SC
F
B
A
LoadCell
HEIGHT ACTUATOR
2,59
Horizontal reaction BEAM
Hydraulic cylinders

(a)

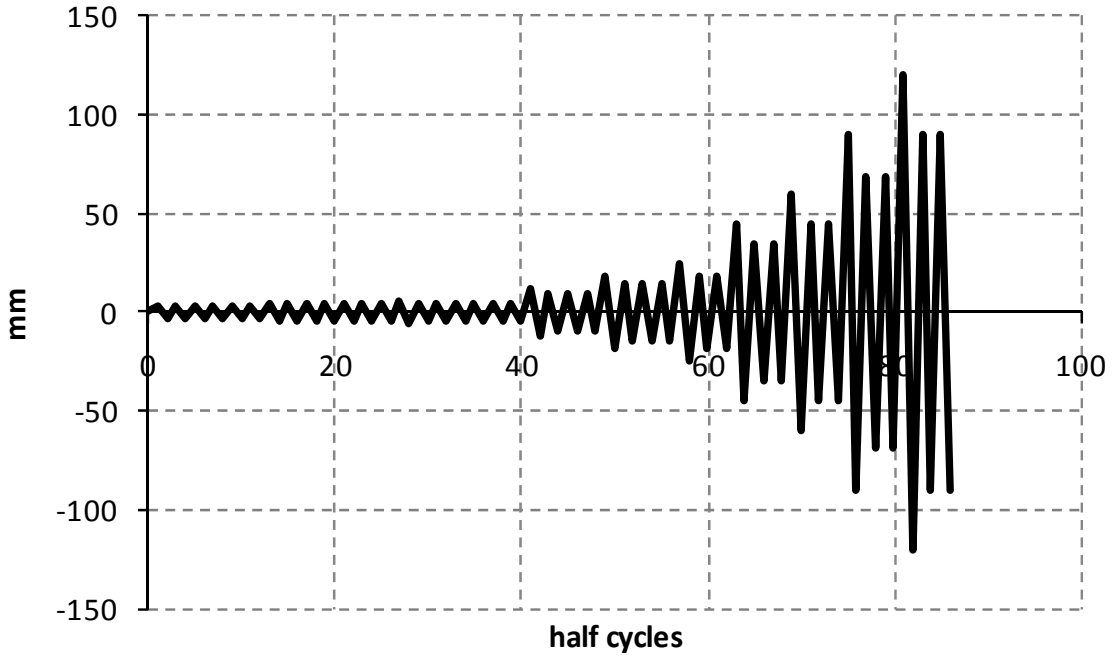
150
100
50
0
-50
-100
-150
mm
0
20
40
60
80
100
half cycles

(b)

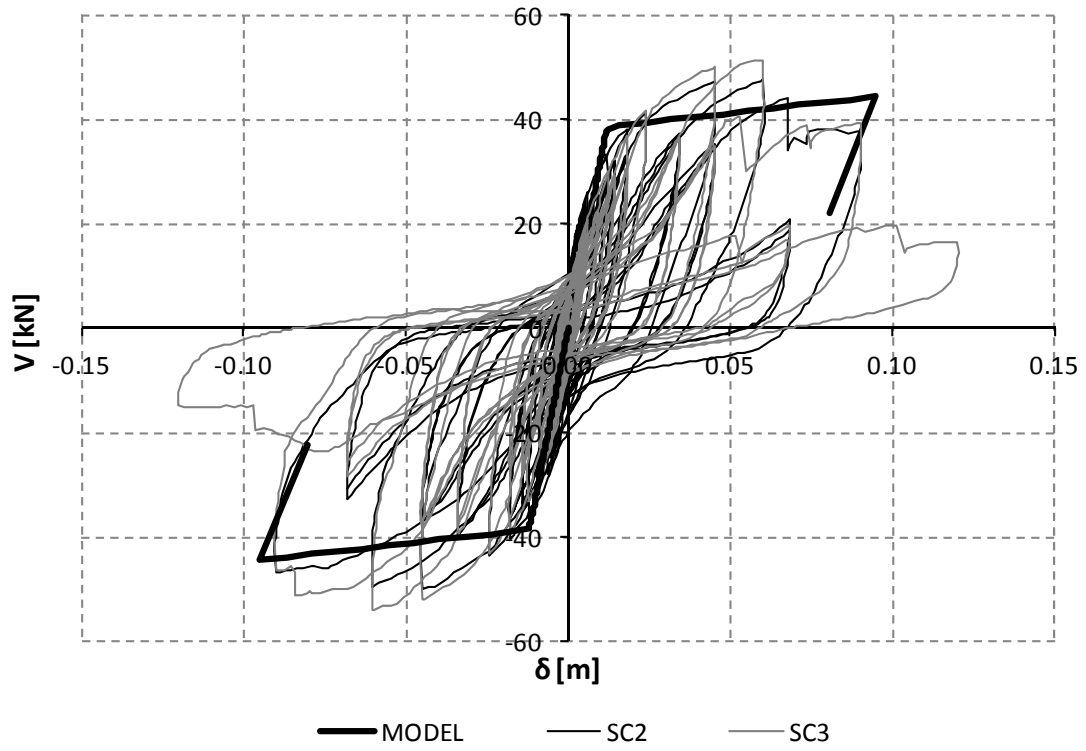


(c)

**Figure 26. (a) Experimental set-up of the IST specimens and (b) applied loading protocol** [25], **and (c) comparison of the pushover curves with the analytical results for SC2 and SC3 specimens.**

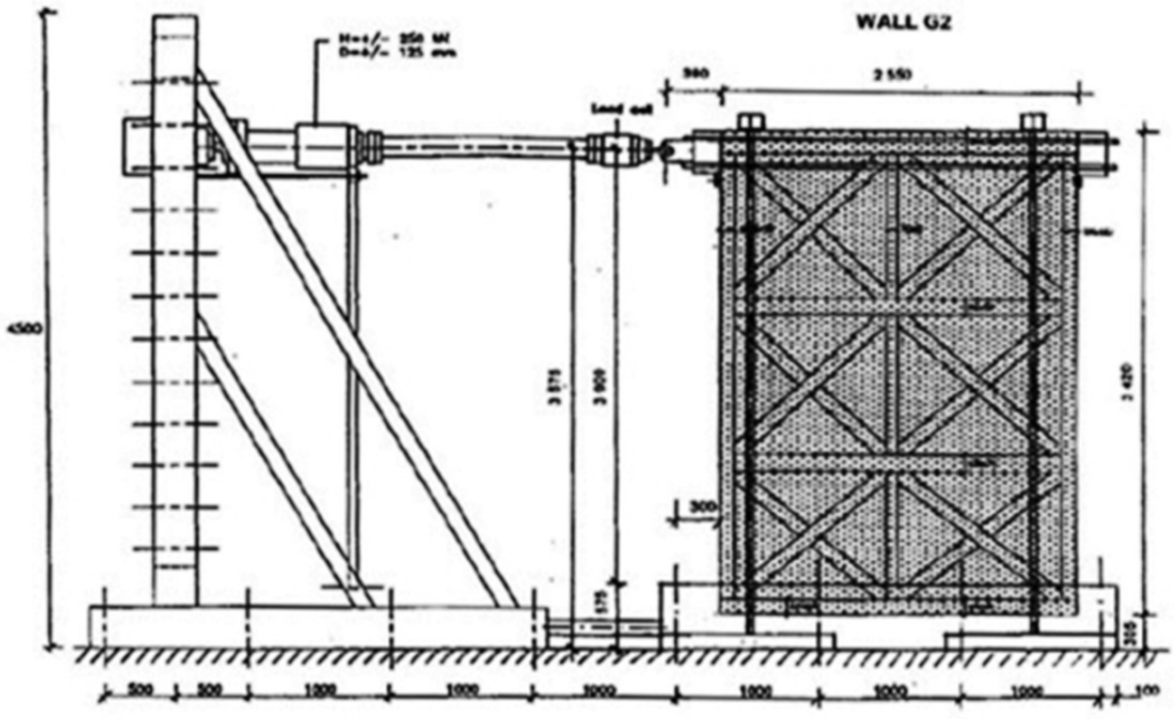
WALL G2

(a)

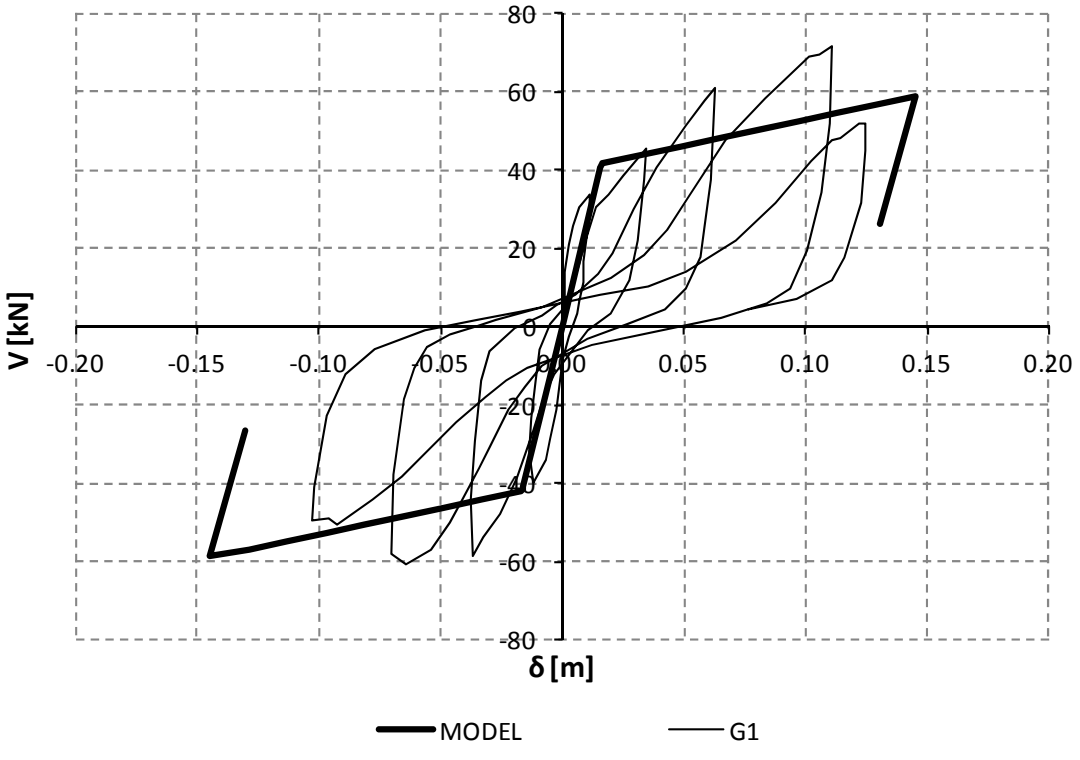
80
60
40
20
0
-20
-40
-60
-80
-0.20
-0.15
-0.10
-0.05
0.00
0.05
0.10
0.15
0.20
V [kN]
δ [m]
MODEL
G1

(b)

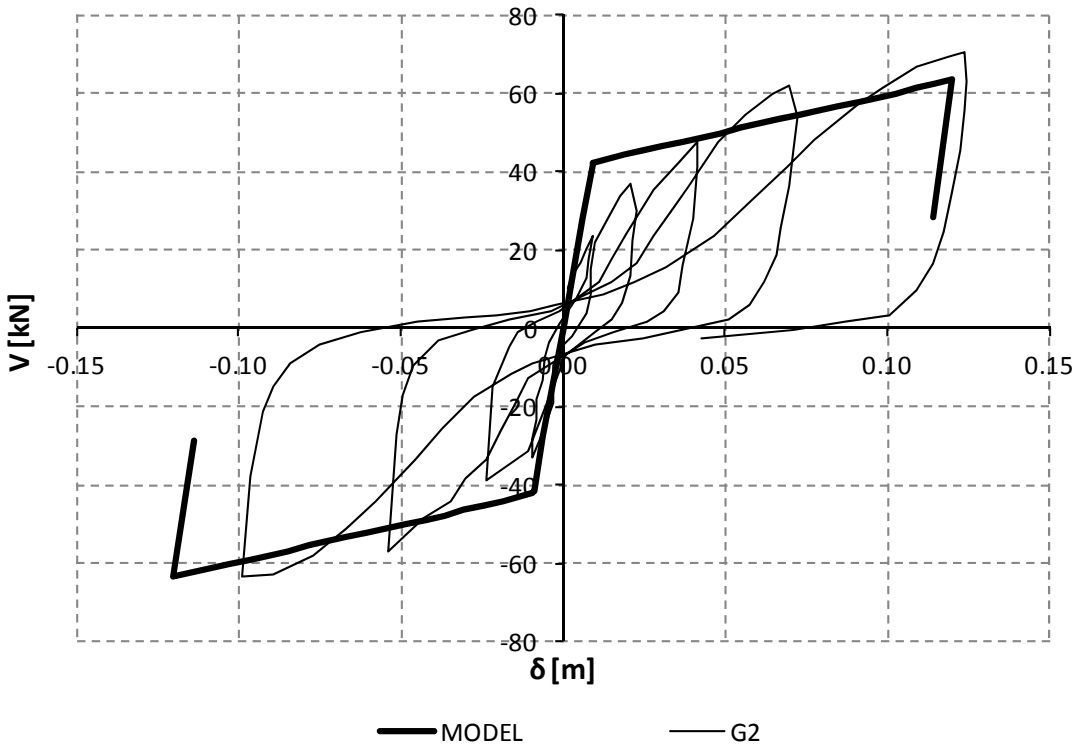


(c)

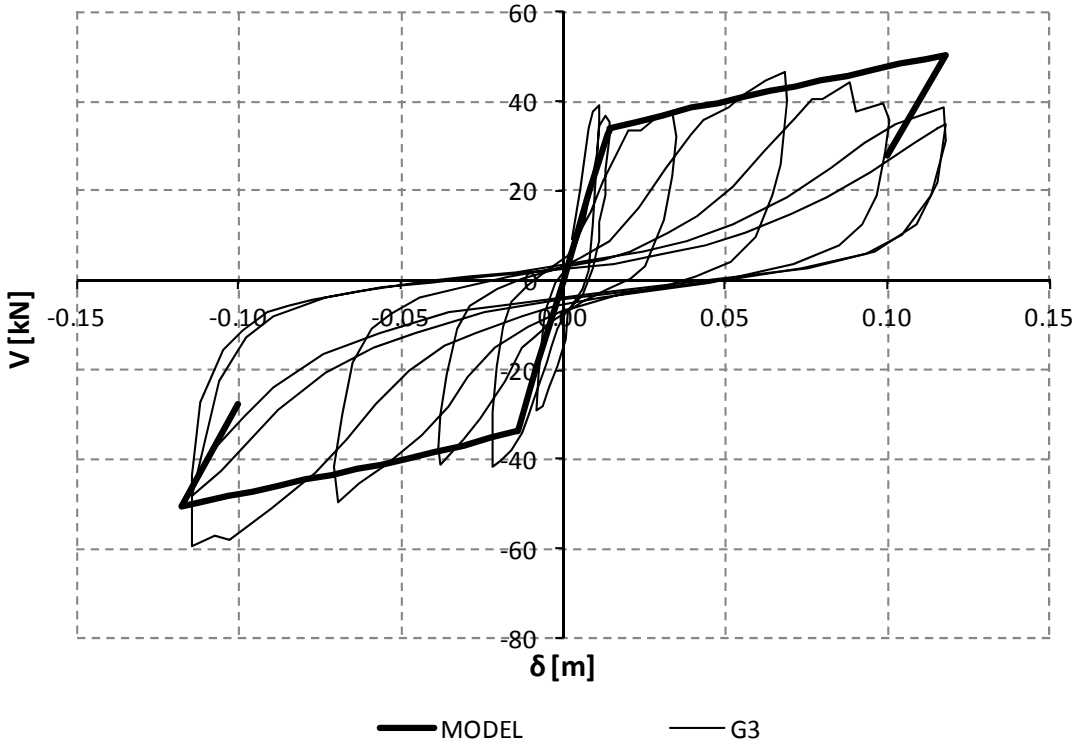


(d)

**Figure 27. (a) Experimental set-up of the LNEC specimens** [6] **and comparison with the analytical results for (b) G1, (c) G2 and (d) G3 specimens.**